

Invariants for Homology Classes with Application to Optimal Search and Planning Problem in Robotics

Subhrajit Bhattacharya David Lipsky Robert Ghrist Vijay Kumar

Abstract

We consider planning problems on a punctured Euclidean spaces, $\mathbb{R}^D - \tilde{\mathcal{O}}$, where $\tilde{\mathcal{O}}$ is a collection of obstacles. Such spaces are of frequent occurrence as configuration spaces of robots, where $\tilde{\mathcal{O}}$ represent either physical obstacles that the robots need to avoid (e.g., walls, other robots, etc.) or illegal states (e.g., all legs off-the-ground). As state-planning is translated to path-planning on a configuration space, we collate equivalent plannings via topologically-equivalent paths. This prompts finding or exploring the different homology classes in such environments and finding representative optimal trajectories in each such class.

In this paper we start by considering the problem of finding a complete set of easily computable homology class invariants for $(N - 1)$ -cycles in $(\mathbb{R}^D - \tilde{\mathcal{O}})$. We achieve this by finding explicit generators of the $(N - 1)^{st}$ de Rham cohomology group of this punctured Euclidean space, and using their integrals to define cocycles. The action of those dual cocycles on $(N - 1)$ -cycles gives the desired complete set of invariants. We illustrate the computation through examples.

We further show that, due to the integral approach, this complete set of invariants is well-suited for efficient search-based planning of optimal robot trajectories with topological constraints. Finally we extend this approach to computation of invariants in spaces derived from $(\mathbb{R}^D - \tilde{\mathcal{O}})$ by collapsing subspace, thereby permitting application to a wider class of non-Euclidean ambient spaces.

1 Introduction

1.1 Motivation: Robot Path Planning with Topological Constraints

In numerous robotics applications, it is important to distinguish between configuration space paths in different topological classes, as a means of categorizing continuous families of plans. This motivation — connected components of paths relative to endpoints — leads to classifying up to homotopy. Examples motivating a classification of homotopy classes of paths include: (1) group exploration of an environment [5], in which an efficient strategy involves allocating one agent per homotopy class; (2) visibility, especially in the tracking of uncertain agents in an environment with dynamic obstacles [19]; and (3) multi-agent coordination, in which (Pareto-) optimal planning coincides with homotopy classification [11].

Although homotopy is a natural topological equivalence relation for paths, the computational bottlenecks involved, especially in higher dimensional configuration spaces, present severe challenges in solving practical problems in robot path planning. Thus we resort to its computationally-simpler cousin — homology (Figure 1). We assume a basic familiarity with first-year algebraic topology, as in [13] for homology and [4] for differential forms and de Rham cohomology.

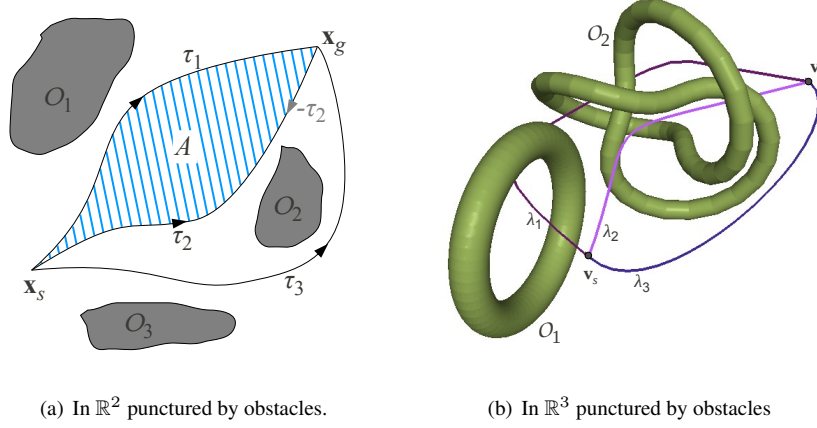


Figure 1: Homology classes of robot trajectories in Euclidean spaces with obstacles.

The methods we employ, following [3], construct an explicit differential 1-form, the integration of which along trajectories gives complete homology class invariants. Such 1-forms are elements of the de Rham cohomology group of the configuration space, $H_{dR}^1(\mathbb{R}^D - \tilde{\mathcal{O}})$. To deal with the obstacles, we replace \mathcal{O} with topologically equivalent codimension-2 skeleta (e.g., Figure 2) and then compute the degrees (or *linking numbers*) of closed loops with the skeleta.

1.2 Contributions of this Paper

We generalize the path-planning problem to higher homology classes and linking numbers of arbitrary submanifolds (not merely 1-dimensional curves representing trajectories). In particular, we will consider $(N - 1)$ -dimensional closed manifolds as generalization of 1-dimensional curves that constituted the trajectories. Obstacles will be represented by codimension N closed manifolds (which, in many cases will be deformation retracts of the original obstacles).

Degree and linking numbers are closely related to homology [13, 7]. We will in fact show that the proposed integration along trajectories give homology class invariants for closed loops (something that was claimed in [3], but not proved rigorously).

The primary aim of this paper is two-fold:

1. To find certain differential $(N - 1)$ -forms in the Euclidean space punctured by obstacles, and show that integration of the forms along $(N - 1)$ -dimensional closed manifolds give a *complete set of invariants* for homology classes of the manifolds in the punctured space (*i.e.* the value of the integral over two closed manifolds are equal if and only if the manifolds are homologous),
2. To adapt and extend the tools used in [3] for robot path planning with topological reasoning to arbitrary dimensional Euclidean configuration spaces punctured by obstacles.

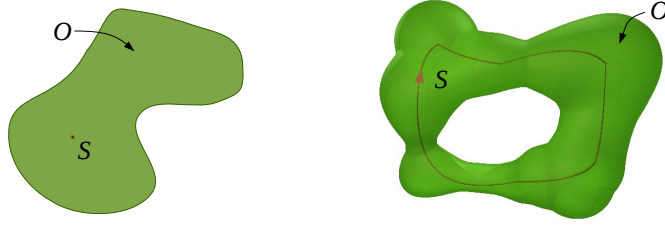


Figure 2: Obstacles, O , can be replaced by equivalents, S , without change to H_{N-1} of the complement.

1.3 Overview and Organization of this Paper

The main concept behind the treatment in this paper is to exploit the pairing $H^{N-1}(\mathbb{R}^D - \tilde{O}; \mathbb{G}) \otimes H_{N-1}(\mathbb{R}^D - \tilde{O}; \mathbb{G}) \rightarrow \mathbb{G}$, which evaluates $(N-1)$ -cocycles over $(N-1)$ -cycles. Given a cycle $\bar{\omega} \in Z_{N-1}(\mathbb{R}^D - \tilde{O}; \mathbb{G})$, and a large enough set of cocycles, $\mathcal{A} = \{\alpha_1, \alpha_2, \dots, \alpha_m\}$, $\alpha_i \in Z^{N-1}(\mathbb{R}^D - \tilde{O}; \mathbb{G})$, one can hope that the set of values $\{\alpha_1(\bar{\omega}), \alpha_2(\bar{\omega}), \dots, \alpha_m(\bar{\omega})\} \in \mathbb{G}^m$ will provide some information about the homology class of $\bar{\omega}$, that is the value of $[\bar{\omega}] \in H_{N-1}(\mathbb{R}^D - \tilde{O}; \mathbb{G})$. In fact choosing the coefficients in \mathbb{R} , and with some assumptions on \tilde{O} , we will show that it is sufficient to choose the elements of \mathcal{A} such that their cohomology classes generate $H^{N-1}(\mathbb{R}^D - \tilde{O}; \mathbb{R})$.

However, the challenge lies in explicitly finding the cochains, α_i , that will serve our purpose and are easy to evaluate on cycles. Due to De Rham's theorem, the cocycles, α_i , can be represented by some $(N-1)$ -form, $\phi_i \in \Omega^{N-1}(\mathbb{R}^D - \tilde{O})$, so that the evaluation of the cocycle over a cycle is, precisely, integration of the form over the cycle. In order to find this form, we exploit the difference map $p : (\mathbb{R}^D - \tilde{O}) \times \tilde{O} \rightarrow (\mathbb{R}^D - \{0\})$. The codomain of this map is the D -dimensional Euclidean space with the origin removed, and is much simpler and well-studied. Thus, if $\eta_0 \in \Omega^{D-1}(\mathbb{R}^D - \{0\})$ is a differential $(D-1)$ -form in $(\mathbb{R}^D - \{0\})$, a simple pull-back via p gives the form $\eta = p^*\eta_0 \in \Omega^{D-1}(\mathbb{R}^D - \tilde{O}) \times \tilde{O}$. Upon integration of η over some $(D-N)$ -cycle, \bar{S} , one may hope to obtain the desired $(N-1)$ -form, $\phi_i = \int_{\bar{S}} p^*\eta_0$. Considering the space $(\mathbb{R}^D - \tilde{O}) \times \tilde{O}$ as a fiber bundle over $(\mathbb{R}^D - \tilde{O})$ with \tilde{O} as the fibers, one may be tempted to integrate $p^*\eta_0$ over the fibers. However, the nature of \tilde{O} (its topology, dimensionality) can be quite arbitrary in general.

Thus we begin by constructing a suitable skeleton \tilde{S} with which to replace \tilde{O} , so that the spaces $(\mathbb{R}^D - \tilde{O})$ and $(\mathbb{R}^D - \tilde{S})$ are identical as far as their $(N-1)^{th}$ homology groups are concerned. However, in that construction, we will ensure that \tilde{S} is a collection (disjoint union) of codimension- N manifolds, thus simplifying the problem.

Throughout this paper we consider homology and cohomology with coefficients in the field \mathbb{R} . As a consequence, all the homology and cohomology groups are freely and finitely generated. Also, for simplicity, we will throughout consider $N > 1$ to avoid the special treatment of the 0^{th} (co)homology groups. All topological spaces referred to in this paper are assumed to be Hausdorff.

2 On Building Obstacle Equivalents

As preparation for the technical details involving linking numbers, we consider the replacement of our obstacles with their $(D-N)$ -dimensional representatives. This is trivial for contractible obstacles in the plane (point representatives) and in 3-dimensional space (cf. the *skeletons* of [3]).

The intuition is that replacing obstacles by their homotopy equivalents leaves the homology classes of trajectories in the complement unchanged (Figure 2); however, we have dimension constraints, and there exist simple obstacles that do not have a $(D - N)$ -dimensional deformation retract (e.g. for the $D = 3, N = 2$ case, a hollow torus does not have a $D - N = 1$ dimensional homotopy equivalent). We therefore turn to $(D - N)$ -dimensional equivalents faithful to homology in the desired dimension (Figure 4).

In the proposition and related corollaries that follow, we represent the ambient configuration space (without obstacles) by \mathbb{R}^D , an obstacle by O , and S the $(D - N)$ -dimensional equivalent of the obstacle with which we replace O for computational simplicity.

Proposition P1. *Let O be a compact, locally contractible subspace of \mathbb{R}^D . Let S be a compact, locally contractible subspace of O , such that the inclusion $i: S \hookrightarrow O$ induces an isomorphism $i_*: H_{D-N}(S) \rightarrow H_{D-N}(O)$. Then the inclusion map $\tilde{i}: (\mathbb{R}^D - O) \hookrightarrow (\mathbb{R}^D - S)$ induces an isomorphism $\tilde{i}_*: H_{N-1}(\mathbb{R}^D - O) \rightarrow H_{N-1}(\mathbb{R}^D - S)$.*

Proof.

Consider the following diagram.

$$\begin{array}{ccccc} H^{D-N}(O) & \xrightarrow{f} & H_N(\mathbb{R}^D, \mathbb{R}^D - O) & \xrightarrow{\partial} & H_{N-1}(\mathbb{R}^D - O) \\ \downarrow i_* & & \downarrow \tilde{i}_* & & \downarrow \tilde{i}_* \\ H^{D-N}(S) & \xrightarrow{f} & H_N(\mathbb{R}^D, \mathbb{R}^D - S) & \xrightarrow{\partial} & H_{N-1}(\mathbb{R}^D - S) \end{array}$$

The vertical arrows are induced by the inclusions i and \tilde{i} . The arrows labeled f are the isomorphisms given by proposition 3.46 of [13] (it is here that we use the hypotheses that O and S be compact and locally contractible). The arrows labeled ∂ are the boundary homomorphisms in the long exact sequence for the pairs $(\mathbb{R}^D, \mathbb{R}^D - O)$ and $(\mathbb{R}^D, \mathbb{R}^D - S)$. These are also isomorphisms, by the contractibility of \mathbb{R}^D .

The square on the right commutes by the naturality of the long exact sequence. The square on the left commutes as well, and while this is not explicitly stated in [13], it follows easily from the proof of Proposition 3.46, *ibid.*

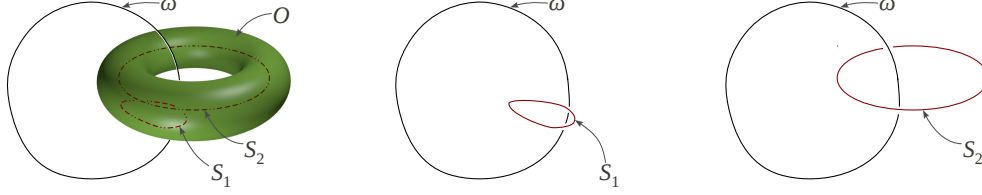
The vertical arrow on the left is an isomorphism by hypothesis (using the Universal Coefficient Theorem over \mathbb{R}), and all the horizontal arrows are isomorphisms, so the vertical arrow on the right must also be an isomorphism.

■

In light of robot path planning, O in the above proposition is a solid obstacle in the environment, and S is its equivalent/replacement (in the terminology of [3] these are *representative points* of obstacles on a 2-dimensional plane, and *skeletons* of obstacles in a 3-dimensional Euclidean space). The aim of the above proposition is to establish a relationship between the homology groups of the complement (or free) spaces, $(\mathbb{R}^D - O)$ and $(\mathbb{R}^D - S)$, from some known relationship between the spaces O and S . In the corollaries below, we suggest couple of approaches for identifying valid replacements, S , of a given obstacles, O .

The following is trivial, but stated formally for future reference.

Corollary C1. *If S and O are compact, locally contractible subspaces of \mathbb{R}^D such that S is a deformation retract of O , then the inclusion map $\tilde{i}: (\mathbb{R}^D - O) \hookrightarrow (\mathbb{R}^D - S)$ induces isomorphisms $\tilde{i}_*: H_*(\mathbb{R}^D - O) \rightarrow H_*(\mathbb{R}^D - S)$*



(a) Both S_1 and S_2 are subsets of the solid torus, O . Moreover, each has the homotopy type of the solid torus. ω is a non-trivial cycle in $(\mathbb{R}^3 - O)$.

(b) $(\mathbb{R}^3 - S_1)$ has homology groups isomorphic to those of $(\mathbb{R}^3 - O)$. However, the cycle ω becomes trivial in $(\mathbb{R}^3 - S_1)$. Thus S_1 is not a valid replacement of O .

(c) $(\mathbb{R}^3 - S_2)$ also has homology groups isomorphic to those of $(\mathbb{R}^3 - O)$. Moreover, the cycle ω remain non-trivial in $(\mathbb{R}^3 - S_2)$. S_2 is a valid replacement of O .

Figure 3: A solid torus [left] with valid [right] and invalid [middle] equivalents. This is an example with $D = 3, N = 2$. The replacement needs to be such that the inclusion map $\tilde{i} : (\mathbb{R}^D - O) \hookrightarrow (\mathbb{R}^D - S)$ induces the isomorphism.

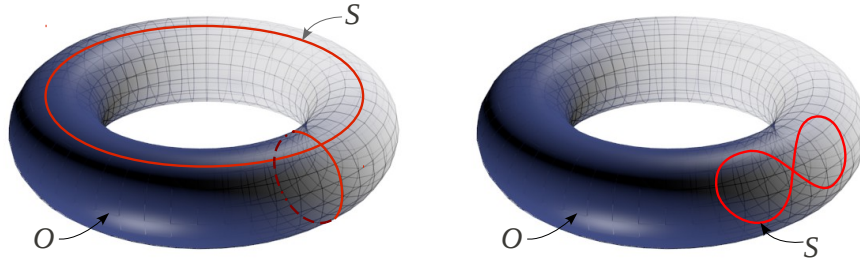


Figure 4: A hollow (or thickened) torus as an obstacle in a $D = 3$ dimensional space, with $N = 2$ for the problem of robot path planning (*i.e.* we are interested in homology classes of $(N - 1) = 1$ -dimensional manifolds, which are closed trajectories). It does not have a $(D - N) = 1$ -dimensional deformation retract or homotopy equivalent. However, we can replace it by its generating 1-cycles (left). Other choices (right) are invalid, when $H_{D-N}(O, S) \not\cong 0$.

Corollary C2. *Let $O \subset \mathbb{R}^D$ be compact and locally contractible. Suppose there exists a set of pairwise-disjoint, connected, closed, oriented $(D - N)$ -dimensional manifolds $S_k \subseteq O$, $k = 1, \dots, m$, such that the fundamental classes $[S_1], \dots, [S_m]$ form a basis for the homology group $H_{D-N}(O)$. Let $\tilde{S} = \bigcup_{k=1}^m S_k$. Then the inclusion map $\tilde{i} : (\mathbb{R}^D - O) \hookrightarrow (\mathbb{R}^D - \tilde{S})$ induces an isomorphism $\tilde{i}_{*,N-1} : H_{N-1}(\mathbb{R}^D - O) \rightarrow H_{N-1}(\mathbb{R}^D - \tilde{S})$.*

Proof.

By construction, the inclusion induces an isomorphism $H_{D-N}(\tilde{S}) \rightarrow H_{D-N}(O)$, and so the result follows from Proposition P1. ■

The consequence of the last two corollaries is that instead of computing homology classes of $(N - 1)$ cycles in the original punctured space $(X - O)$, we can replace the obstacles O with equivalents S while preserving the relevant homology (cf. [3] for special cases). In cases where $(D - N)$ -dimensional deformation retracts do not exist (e.g., Figure 4), Corollary C2 allows one to replace obstacles by $(D - N)$ -dimensional equivalents (generating cycles of $(D - N)^{th}$ homology group).

2.1 Reduced Problem Definition

Thus we have established that obstacles $\tilde{O} \subset \mathbb{R}^D$ (which represent illegal zones in robot planning problems) may be replaced by equivalents \tilde{S} preserving the appropriate homology. We may (and do) choose the equivalents \tilde{S} to be a disjoint union of connected, closed, orientable $(D - N)$ -dimensional manifolds. The reduced problem definition follows:

Given: (1) the *singularity manifolds* — a disjoint collection $\tilde{S} = S_1 \sqcup S_2 \sqcup \dots \sqcup S_m$ of $(D - N)$ -dimensional ($N > 1$), connected, closed, orientable submanifolds, of \mathbb{R}^D ; and (2) the *candidate manifolds* — a collection of $(N - 1)$ -dimensional, closed, orientable manifolds in $(\mathbb{R}^D - \tilde{S})$.

Problem: identify the homology classes of the candidate manifolds in the complement of the singularity manifolds. Specifically, design a complete set of easily-computed invariants for these homology classes by finding a set of explicit generators for $H^{N-1}(\mathbb{R}^D - \tilde{S})$ and integrating these generators over candidate manifolds.

In order to compute the action of the cocycles on the candidate manifolds, we represent them as $(N - 1)$ -cycles (*i.e.* top-dimensional covering cycles). Thus, given a candidate manifold ω , we can use a *cellular cover* of the manifold, $\bar{\omega}$, which is also an $(N - 1)$ -cycle in $(\mathbb{R}^D - \tilde{S})$ under the inclusion map $\omega \hookrightarrow (\mathbb{R}^D - \tilde{S})$ (a map that we will assume implicitly most often). However, given two cycles $\bar{\omega}_1, \bar{\omega}_2 \in Z_{N-1}(\mathbb{R}^D - \tilde{S})$, instead of checking if or not $\bar{\omega}_1 - \bar{\omega}_2$ is boundary in $H_{N-1}(\mathbb{R}^D - \tilde{S})$, we will compute complete invariants $\phi_{\tilde{S}}(\bar{\omega}_1)$ and $\phi_{\tilde{S}}(\bar{\omega}_2)$, comparing them to make the desired assertion. In particular, we construct the function $\phi_{\tilde{S}}(\cdot)$ to be in form of an integration over $\bar{\omega}$ of some set of differential $(N - 1)$ -forms. Our strategy — using integration and differential forms — is a traditional method for understanding (co)homology of manifolds and submanifolds [4].

3 Preliminaries on Linking Numbers

Equipped with the notion of the $(D - N)$ -dimensional replacements of the obstacles/punctures, S_i , we proceed towards computing the homology classes of $(N - 1)$ -cycles (in light of robot planning

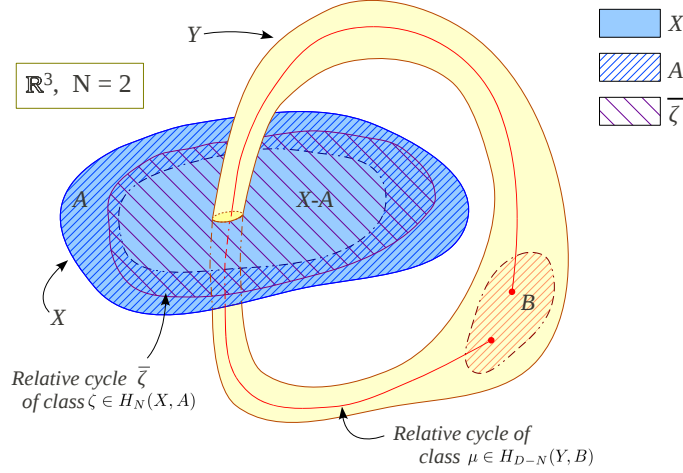


Figure 5: Illustration of intersection number in \mathbb{R}^3 with $N = 2$ in light of Definition D1.

problem those are the closed trajectories) of $(\mathbb{R}^D - \tilde{S})$. In this section we recall various notions of *intersection* and *linking number*, and from this:

- i. Infer homology classes of the $(N - 1)$ -cycles in $(\mathbb{R}^D - S_i)$ from linking data (Proposition P3),
- ii. Computing the linking number using an integration over the $(N - 1)$ -cycle and a top-dimensional cycle of the S_i (Proposition P4).

We illustrate the ideas using examples from robot planning problems.

3.1 Definitions

Recall the definition of *intersection number*:

Definition D1 (Intersection Number – Ch. VII, Def. 4.1 of [7]). Suppose X and Y are submanifolds of \mathbb{R}^D , and $A \subset X \subset \mathbb{R}^D$, $B \subset Y \subset \mathbb{R}^D$ are such that $A \cap Y = \emptyset$, $X \cap B = \emptyset$ (Figure 5). Consider the map $p : (X \times Y, A \times Y \cup X \times B) \rightarrow (\mathbb{R}^D, \mathbb{R}^D - \{0\})$ given by $p(x, y) = x - y$. The composition

$H_N(X, A) \times H_{D-N}(Y, B) \xrightarrow{\times} H_D(X \times Y, A \times Y \cup X \times B) \xrightarrow{(-1)^{D-N} p_*} H_D(\mathbb{R}^D, \mathbb{R}^D - \{0\})$ is called the *intersection pairing* (where ' \times ' denotes the homology cross product – see p. 268 of [13]). We write

$$\mathcal{I}(\zeta, \mu) = (-1)^{D-N} p_*(\zeta \times \mu), \quad \text{for } \zeta \in H_N(X, A), \mu \in H_{D-N}(Y, B)$$

and call this element of $H_D(\mathbb{R}^D, \mathbb{R}^D - \{0\}) \cong \mathbb{R}$ the *intersection number* of ζ and μ .

Definition D2 (Linking Number – Adapted from Ch. 10, Art. 77 of [16]). We borrow definitions of X, A, Y and B from Definition D1. Recall from the *long exact sequence* of the pair (X, A) the *connecting homomorphism* $\partial_* : H_N(X, A) \rightarrow H_{N-1}(A)$. If $\varsigma \in H_{N-1}(A)$ is such that it can be written as $\varsigma = \partial_* \zeta$ for some $\zeta \in H_N(X, A)$, and if $\mu \in H_{D-N}(Y, B)$, then the *linking number* between ς and μ is defined as $\mathcal{L}(\varsigma, \mu) = \mathcal{I}(\zeta, \mu)$.

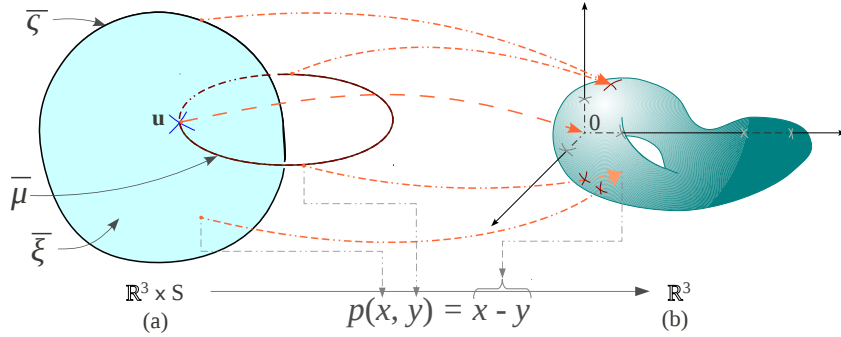


Figure 6: A simplified illustration (following from Figure 3(c)) of intersection number and linking number in \mathbb{R}^3 with $N = 2$. This is a special case of Definition D1 when $X = \mathbb{R}^3$, $A = \mathbb{R}^3 - S$, $Y = S$ and $B = \emptyset$. *Figure (a) on the left:* The intersection number is computed between a N -chain, $\bar{\xi}$ (more precisely it is a relative cycle in (X, A) that we consider – the boundary of $\bar{\xi}$ trivialized), and the $(D - N)$ -cycle, $\bar{\mu}$, that is a top-dimensional cycle on S . In this figure the said intersection number is ± 1 due to the single intersection marked by the ‘cross’ at u . Then, by definition, that is equal to the linking number between $\bar{\zeta} = \partial \bar{\xi}$ and $\bar{\mu}$. *Figure (b) on the right:* The precise definition requires a mapping, p , from pair of points in the original space (one point from the 2-chain, $\bar{\xi}$, embedded in the ambient space, \mathbb{R}^3 , and another from S) to (a different copy of) \mathbb{R}^3 . The intersection/linking number is then, informally, the number of times intersection points in the pre-image of p (points like u) maps to the origin, 0 (with proper sign), in the image, or equivalently, the number of times the image of $\bar{\zeta} \times \bar{\mu}$, under the action of p , wraps around the origin. Thus, it is the homology class of the cycle $p(\bar{\zeta} \times \bar{\mu})$ in the punctured Euclidean space $(\mathbb{R}^D - 0)$.

3.2 Propositions on Linking Number

We state and two propositions. The first is well-known but stated for completeness.

Proposition P2 (Uniqueness of linking number). *If $H_N(X) = H_{N-1}(X) = 0$ holds, then $\mathcal{L}(\zeta, \mu)$ is independent of the choice of ζ in Definition D2 [16].*

Proposition P3 (Connection to homology of A). *Consider a fixed non-zero $\mu \in H_{D-N}(Y, B)$. If, in addition to the condition of Proposition P2, we have $H_N(X, A) \cong H_{N-1}(A) \cong \mathbb{R}$, and if there exists at least one $(N - 1)$ -cycle in A such that its linking number with μ is non-zero, then the value of $\mathcal{L}(\zeta, \mu)$ tells us which element of $H_{N-1}(A)$ is the chosen ζ . In other words, the map $\mathcal{H} \equiv \mathcal{L}(\cdot, \mu) : H_{N-1}(A) \rightarrow H_{D-1}(\mathbb{R}^D, \mathbb{R}^D - \{0\}) \cong \mathbb{R}$ is an injective homomorphism.*

Proof.

The map \mathcal{H} is given by $\mathcal{H}(\zeta) = (-1)^{D-N} p_*(\partial_*^{-1} \zeta \times \mu)$. This clearly is a group homomorphism between $H_{N-1}(A)$ and $H_{D-1}(\mathbb{R}^D, \mathbb{R}^D - \{0\})$. Since by hypothesis, both the domain and the co-domain of \mathcal{H} are isomorphic to \mathbb{R} , \mathcal{H} can either be a trivial homomorphism (*i.e.* maps everything in its domain to 0 in its co-domain), or it can be an injection. The former possibility is ruled out by the hypothesis of existence of at least one $(N - 1)$ -cycle in A with non-zero linking number with μ . Thus the result follows. ■

The result implies that the linking number with μ is a *complete invariant* for the homology class ζ .

3.3 Computation of Intersection/Linking Number for Given Cycles

We describe how to compute the linking number between the cycles $\bar{\varsigma}$ and $\bar{\mu}$. As discussed in the beginning of this paper, we would like to be able to compute the homology class of $(N-1)$ -cycles (top-dimensional cycles on $(N-1)$ -dimensional manifolds) as an explicit number (or a set of numbers). Equipped with Proposition P3, that problem can be converted to the problem of computation of the linking numbers.

Let $\eta_0 \in \Omega_{dR}^{D-1}(\mathbb{R} - \{0\})$ be a closed differential form that represents the standard generator of $H^{D-1}(\mathbb{R}^D - \{0\})$. Let $j_*: H_{D-N}(Y) \rightarrow H_{D-N}(Y, B)$ denote the quotient map.

Proposition P4. *Assume the same hypotheses as in Proposition P2. Fix $\mu \in H_{D-N}(Y, B)$, and suppose there exists a class $u \in H_{D-N}(Y)$ such that $j_*(u) = \mu$. Then for any $\varsigma \in H_{N-1}(A)$, the linking number $\mathcal{L}(\varsigma, \mu)$ is uniquely determined by the value of the integral*

$$(-1)^{D-N} \int_{\varsigma \times u} p^*(\eta_0). \quad (1)$$

Proof.

First, note that the map

$$H_D(\mathbb{R}^D, \mathbb{R}^D - \{0\}) \xrightarrow{\partial_*} H_{D-1}(\mathbb{R}^D - \{0\}) \xrightarrow{\int \cdot \eta_0} \mathbb{R}$$

is an isomorphism, so that every element $m \in H_D(\mathbb{R}^D, \mathbb{R}^D - \{0\})$ is uniquely determined by the value of the integral $\int_{\partial_* m} \eta_0$.

Choose a class $\zeta \in H_N(X, A)$ such that $\partial_*(\zeta) = \varsigma$. Then, by definition,

$$\mathcal{L}(\varsigma, \mu) = \mathcal{J}(\zeta, \mu) = (-1)^{D-N} p_*(\zeta \times \mu) \in H_D(\mathbb{R}^D, \mathbb{R}^D - \{0\}).$$

Now, consider the diagram below.

$$\begin{array}{ccccc}
 & & H_N(X, A) \otimes H_{D-N}(Y) & & \\
 & \swarrow 1 \otimes j_* & \downarrow \times & \searrow \partial_* \otimes 1 & \\
 H_N(X, A) \otimes H_{D-N}(Y, B) & & H_D(X \times Y, A \times Y) & & H_{N-1}(A) \otimes H_{D-N}(Y) \\
 \downarrow \times & \swarrow j_* & \downarrow p_* & \searrow \partial_* & \downarrow \times \\
 H_D(X \times Y, A \times Y \cup X \times B) & & H_D(\mathbb{R}^D, \mathbb{R}^D - \{0\}) & & H_{D-1}(A \times Y) \\
 \searrow p_* & & \downarrow \partial_* & & \downarrow p_* \\
 & & H_D(\mathbb{R}^D, \mathbb{R}^D - \{0\}) & & H_{D-1}(\mathbb{R}^D - \{0\})
 \end{array}$$

It is a standard fact that every part of this diagram commutes, and as a consequence we have that

$$\partial_* p_*(\zeta \times \mu) = \partial_* p_*(\zeta \times j_* u) = p_*(\partial_* \zeta \times u) = p_*(\varsigma \times u)$$

Finally, by the naturality of integration, we have

$$\int_{\partial_* \mathcal{L}(\varsigma, \mu)} \eta_0 = (-1)^{D-N} \int_{p_*(\varsigma \times u)} \eta_0 = (-1)^{D-N} \int_{\varsigma \times u} p^*(\eta_0).$$

Thus the integral on the right uniquely determines the value of the linking number $\mathcal{L}(\varsigma, \mu)$. ■

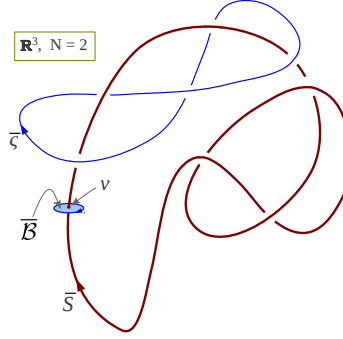


Figure 7: The specific problem under consideration, illustrated for $D = 3, N = 2$.

Note that linking number, by definition, is defined between a cycle in A and a relative cycle in (Y, B) . However, for computing the integration of Equation (1), the cycles we choose are from A and Y . Thus it is possible to use the standard notion of integration over chains [4]. However, if $B = \emptyset$, a relative cycle in (Y, B) becomes a cycle in Y .

4 Construction and Explicit Computation

4.1 Construction of the Complete Invariant

We specialize the results of the previous section to match the description of the *reduced problem definition* in Section 2.1. At present, we consider the case where there is a single path-connected component of \tilde{S} , namely S . In connection to the definitions stated in Section 3 (cf. Figure 6), we set

$$X = \mathbb{R}^D, \quad A = \mathbb{R}^D - S, \quad Y = S \quad \text{and} \quad B = \emptyset$$

Moreover, since $Y \equiv S$ is a $(D - N)$ -dimensional closed, connected and oriented manifold, we have $H_{D-N}(S) \cong \mathbb{R}$. We thus choose $\bar{\mu} = \bar{S} \in Z_{D-N}(S)$ to be a cycle representing the fundamental class of S , i.e. the generator $1 \in H_{D-N}(S)$. Also, note that since $B = \emptyset$, the map $j' : Z_{D-N}(Y) \rightarrow Z_{D-N}(Y, B)$ is the identity map. So in this case $[\bar{S}] \in H_{D-N}(S, B) \equiv H_{D-N}(S)$.

For this choice it is easy to verify that the conditions of Propositions P2, P3 and P4 hold.

i. *Proposition P2*: $H_N(\mathbb{R}^D) = H_{N-1}(\mathbb{R}^D) = 0$ follows from contractibility of \mathbb{R}^D .

ii. *Proposition P3*:

- a. By Alexander duality [13], $H_N(\mathbb{R}^D, \mathbb{R}^D - S) \cong H^{D-N}(S)$. Using Poincaré Duality for S , $H^{D-N}(S) \cong H_0(S) \cong \mathbb{R}$. Finally, from the long exact sequence for the pair $(\mathbb{R}^D, \mathbb{R}^D - S)$, using the contractibility of \mathbb{R}^D , we have, $H_N(\mathbb{R}^D, \mathbb{R}^D - S) \cong H_{N-1}(\mathbb{R}^D - S)$. Combining these three isomorphisms we have,

$$H_N(\mathbb{R}^D, \mathbb{R}^D - S) \cong H_{N-1}(\mathbb{R}^D - S) \cong \mathbb{R} \quad (2)$$

- b. Consider a point $v \in S$. Since \bar{S} covers S , this point is also in (the image of) \bar{S} . Since S is $(D - N)$ -dimensional, we can choose a small N -ball, \mathcal{B} , centered at v such that

it intersects S transversely only at v . Let $\bar{\mathcal{B}} \in C_N(\mathbb{R}^D)$ be a top-dimensional non-zero chain that covers \mathcal{B} . Clearly the intersection number between \bar{S} and $j(\bar{\mathcal{B}})$ (where $j : \mathbb{R}^D \rightarrow \mathbb{R}^D/(\mathbb{R}^D - S)$ is the quotient map) is non-zero. Thus the linking number between $\partial\bar{\mathcal{B}}|_{(\mathbb{R}^D - S)}$ (which, by our construction, is a $(N-1)$ -cycle in $(\mathbb{R}^D - S)$) and \bar{S} is non-zero. Thus there exists at least one $(N-1)$ -cycle in $(\mathbb{R}^D - S)$ that has non-zero linking number with \bar{S} (see Figure 7).

iii. *Proposition P4*: Follows from the fact that $B = \emptyset$.

Construction: A complete invariant for homology classes of $(N-1)$ -cycles, $\bar{\omega} \in Z_{N-1}(\mathbb{R}^D - S)$, is, by Proposition P3, the linking number between $\bar{\omega}$ and \bar{S} . Using Proposition P4, the complete invariant, ϕ_S , for the homology classes of such chains is given by the integral

$$\begin{aligned}\phi_S(\bar{\omega}) &= (-1)^{D-N} \int_{\bar{\omega} \times \bar{S}} p^*(\eta_0) \\ &= (-1)^{D-N} \int_{\bar{\omega}} \int_{\bar{S}} p^*(\eta_0) \quad [\text{Fubini theorem}]\end{aligned}\quad (3)$$

4.2 Computation of ϕ_S

Let $\mathbf{x} \in (\mathbb{R}^D - S) \subset \mathbb{R}^D$ be the coordinate variable describing points in $(\mathbb{R}^D - S)$, and let $\mathbf{x}' \in S \subset \mathbb{R}^D$ be the one describing points in S . Thus we have $p(\mathbf{x}, \mathbf{x}') = \mathbf{x} - \mathbf{x}'$. A well-known [1, 9] explicit generator for the deRham cohomology $H_{dR}^{D-1}(\mathbb{R}^D - \{0\})$ is,

$$\eta_0 = \sum_{k=1}^D \mathcal{G}_k (-1)^{k+1} ds_1 \wedge \cdots \wedge ds_{k-1} \wedge ds_{k+1} \wedge \cdots \wedge ds_D = \sum_{k=1}^D \mathcal{G}_k (-1)^{k+1} \bigwedge_{\substack{i=1 \\ i \neq k}}^D ds_i \quad (4)$$

where,

$$\mathcal{G}_k(\mathbf{s}) = \frac{1}{A_{D-1}} \frac{s_k}{(s_1^2 + s_2^2 + \cdots + s_D^2)^{D/2}} \quad (5)$$

for $\mathbf{s} = (s_i) \in (\mathbb{R}^D - \{0\})$, and $A_{D-1} = \frac{D\pi^{\frac{D}{2}}}{\Gamma(\frac{D}{2}+1)}$, the $(D-1)$ -volume of the $(D-1)$ -dimensional unit sphere.

The pullback of η_0 under p is given by the following formula,

$$\eta(\mathbf{x}, \mathbf{x}') = p^*(\eta_0) = \eta_0|_{\mathbf{s}=\mathbf{x}-\mathbf{x}'} = \sum_{k=1}^D \mathcal{G}_k (-1)^{k+1} \bigwedge_{\substack{i=1 \\ i \neq k}}^D d(x_i - x'_i) \quad (6)$$

Now consider the quantity of interest, $\phi(\bar{\omega}) = \int_{\bar{\omega} \times \bar{S}} \eta(\mathbf{x}, \mathbf{x}')$. On $\bar{\omega} \times \bar{S}$, at most $(N-1)$ unprimed differentials can be independent, and at most $(D-N)$ primed differentials can be independent (since \mathbf{x} represents a point on the image of the $(N-1)$ chain $\bar{\omega}$ and \mathbf{x}' represents a point on the image of the $(D-N)$ chain \bar{S}). Thus we can conveniently drop all the terms in the expansion of η (which is a $(D-1)$ -differential form on $(\mathbb{R}^D - S) \times S$) that do not satisfy these conditions on maximum number of primed/unprimed differentials. Thus we obtain a simpler differential form $\tilde{\eta}$,

$$\tilde{\eta}(\mathbf{x}, \mathbf{x}') = \sum_{k=1}^D \left(\mathcal{G}_k(\mathbf{x} - \mathbf{x}') (-1)^{k+1+D-N} \sum_{\substack{\tau_i \in \{0,1\} \\ \tau_1 + \cdots + \tau_D = D-N}} \bigwedge_{\substack{i=1 \\ i \neq k}}^D dx_i^{(\tau_i)} \right) \quad (7)$$

[where, $x_i^{(\tau)}$ represents x'_i if $\tau = 1$, otherwise represents x_i if $\tau = 0$.]

This differential form, though simpler, has the property that

$$\phi_S(\bar{\omega}) = (-1)^{D-N} \int_{\mathbf{x} \in \bar{\omega}} \int_{\mathbf{x}' \in \bar{S}} \eta(\mathbf{x}, \mathbf{x}') = (-1)^{D-N} \int_{\mathbf{x} \in \bar{\omega}} \int_{\mathbf{x}' \in \bar{S}} \tilde{\eta}(\mathbf{x}, \mathbf{x}') \quad (8)$$

Finally, we re-write the formula for $\tilde{\eta}$ using a new notation as follows,

$$\begin{aligned} \tilde{\eta}(\mathbf{x}, \mathbf{x}') &= (-1)^{D-N} \sum_{k=1}^D \left(\mathcal{G}_k(\mathbf{x} - \mathbf{x}') (-1)^{k+1} \cdot \right. \\ &\quad \left. \sum_{\rho \in \text{part}^{D-N}(\mathcal{N}_{-k}^D)} \text{sgn}(\rho) \, dx'_{\rho_l(1)} \wedge \cdots \wedge dx'_{\rho_l(D-N)} \wedge dx_{\rho_r(1)} \wedge \cdots \wedge dx_{\rho_r(N-1)} \right) \end{aligned} \quad (9)$$

where,

1. $\mathcal{N}_{-k}^D = [1, 2, \dots, k-1, k+1, \dots, D]$ is an ordered set,
2. $\text{part}^w(\mathcal{A})$ is the set of all 2 partitions of the ordered set \mathcal{A} , such that the first partition contains w elements, and each of the partitions contain elements in order. The sign of an element from the set is the permutation sign of the ordered set formed by concatenating the two partitions of the element.

Thus, the final formula for the complete invariant for homology class of $\bar{\omega} \in Z_{N-1}(\mathbb{R}^D - S)$ is,

$$\begin{aligned} \phi_S(\bar{\omega}) &= (-1)^{D-N} \int_{\mathbf{x} \in \bar{\omega}} \int_{\mathbf{x}' \in \bar{S}} \tilde{\eta}(\mathbf{x}, \mathbf{x}') \\ &= \int_{\mathbf{x} \in \bar{\omega}} \sum_{k=1}^D \sum_{\rho \in \text{part}^{D-N}(\mathcal{N}_{-k}^D)} U_{\rho}^k(\mathbf{x}; S) \wedge dx_{\rho_r(1)} \wedge \cdots \wedge dx_{\rho_r(N-1)} \end{aligned} \quad (10)$$

where,

$$U_{\rho}^k(\mathbf{x}; S) = (-1)^{k+1} \text{sgn}(\rho) \int_{\mathbf{x}' \in \bar{S}} \mathcal{G}_k(\mathbf{x} - \mathbf{x}') \, dx'_{\rho_l(1)} \wedge \cdots \wedge dx'_{\rho_l(D-N)} \quad (11)$$

and by convention, \bar{S} is a top-dimensional cycle covering S such that $[\bar{S}] = \mathbf{1} \in H_{D-N}(S)$.

Also, note that the quantity inside the integral in the formula for ϕ_S is a differential $(N-1)$ -form in $(\mathbb{R}^D - S)$. Thus we can integrate it over $\bar{\omega}$. We represent the differential $(N-1)$ -form by ψ_S

$$\psi_S = \sum_{\rho \in \text{part}^{D-N}(\mathcal{N}_{-k}^D)} U_{\rho}^k(\mathbf{x}; S) \wedge dx_{\rho_r(1)} \wedge \cdots \wedge dx_{\rho_r(N-1)} \quad (12)$$

It should be noted that the η_0 we used in (4) is just a particular choice, but this choice is the only symmetric one (up to a scalar multiple) under rotations about the origin. This symmetry enables us to write a clean formula in coordinates, but in general any closed and non-exact form η_0 would work. The resulting invariant would differ from ours by a constant multiple.

4.3 Incorporating Multiple Connected Components of $\tilde{\mathcal{S}}$

So far we have worked in the case of a single connected obstacle S . However, recall that the original space under consideration was $(\mathbb{R}^D - \tilde{\mathcal{S}})$, with $\tilde{\mathcal{S}} = \sqcup_{i=1}^m S_i$, such that each S_i is a path connected, closed, locally contractible and orientable $(D-N)$ -manifold. A straightforward induction argument computes the homology of the smaller space, $(\mathbb{R}^D - \tilde{\mathcal{S}})$, in terms of the larger spaces, $(\mathbb{R}^D - S_k)$.

Proposition P5. $H_{N-1}(\mathbb{R}^D - \tilde{\mathcal{S}}) \cong \bigoplus_{k=1}^m H_{N-1}(\mathbb{R}^D - S_k) \cong \mathbb{R}^m$, where the first isomorphism is induced by the direct sum of the inclusion maps $\tilde{i}_k : (\mathbb{R}^D - \tilde{\mathcal{S}}) \hookrightarrow (\mathbb{R}^D - S_k)$.

Proof.

Recall that the spaces S_i are pairwise disjoint, so that for any p

$$\begin{aligned} (\mathbb{R}^D - S_p) \cup (\mathbb{R}^D - \sqcup_{i=p+1}^m S_i) &= \mathbb{R}^D \\ (\mathbb{R}^D - S_p) \cap (\mathbb{R}^D - \sqcup_{i=p+1}^m S_i) &= \mathbb{R}^D - \sqcup_{i=p}^m S_i \end{aligned}$$

From the Mayer-Vietoris sequence [13] for the triad $(\mathbb{R}^D; \mathbb{R}^D - S_p, \mathbb{R}^D - \sqcup_{i=p+1}^m S_i)$, one obtains an isomorphism

$$H_{N-1}(\mathbb{R}^D - \sqcup_{i=p}^m S_i) \xrightarrow{(\tilde{u}_{p*}, \tilde{v}_{p*})} H_{N-1}(\mathbb{R}^D - S_p) \oplus H_{N-1}(\mathbb{R}^D - \sqcup_{i=p+1}^m S_i) \quad (13)$$

Note that $\tilde{u}_{1*} = \tilde{i}_{1*}$ and, $\tilde{v}_{1*} \circ \tilde{v}_{2*} \circ \dots \circ \tilde{v}_{(p-1)*} \circ \tilde{u}_{p*} = \tilde{i}_{p*}$.

By induction on p , we obtain a sequence of isomorphisms

$$\begin{aligned} H_{N-1}(\mathbb{R}^D - \tilde{\mathcal{S}}) &\xrightarrow{(\tilde{i}_{1*}, \tilde{v}_{1*})} H_{N-1}(\mathbb{R}^D - S_1) \oplus H_{N-1}(\mathbb{R}^D - \sqcup_{i=2}^m S_i) \\ &\xrightarrow{(\tilde{i}_{1*}, \tilde{i}_{2*}, \tilde{v}_{2*})} H_{N-1}(\mathbb{R}^D - S_1) \oplus H_{N-1}(\mathbb{R}^D - S_2) \oplus H_{N-1}(\mathbb{R}^D - \sqcup_{i=3}^m S_i) \\ &\quad \dots \\ &\xrightarrow{\bigoplus_{k=1}^m \tilde{i}_{k*}} \bigoplus_{k=1}^m H_{N-1}(\mathbb{R}^D - S_k) \end{aligned} \quad (14)$$

The fact that this is isomorphic to \mathbb{R}^m follows from Equation (2), where we showed $H_{N-1}(\mathbb{R}^D - S_k) \cong \mathbb{R}$. \blacksquare

The following theorem hence follows directly from Propositions P5 and Equation (3).

Theorem T1. For any $\bar{\omega} \in Z_{N-1}(\mathbb{R}^D - \tilde{\mathcal{S}})$, a complete invariant for the homology class of $\bar{\omega}$ is given by,

$$\phi_{\tilde{\mathcal{S}}}(\bar{\omega}) \stackrel{def.}{=} \begin{bmatrix} \phi_{S_1}(\bar{\omega}) \\ \phi_{S_2}(\bar{\omega}) \\ \vdots \\ \phi_{S_m}(\bar{\omega}) \end{bmatrix} \quad (15)$$

where, ϕ_{S_i} is given by the formula in Equation (10).

Note that we have implicitly assumed a inclusion map $\tilde{i}_k : (\mathbb{R}^D - \tilde{\mathcal{S}}) \hookrightarrow (\mathbb{R}^D - S_k)$ being applied on $\bar{\omega}$ for computation of the k^{th} component. For simplicity we do not write it explicitly, since the map is identity as far as computation is concerned.

Thus, $[\bar{\omega}_1] = [\bar{\omega}_2]$ if and only if $\phi_{\tilde{\mathcal{S}}}(\bar{\omega}_1) = \phi_{\tilde{\mathcal{S}}}(\bar{\omega}_2)$, for any $\bar{\omega}_1, \bar{\omega}_2 \in Z_{N-1}(\mathbb{R}^D - \tilde{\mathcal{S}})$.

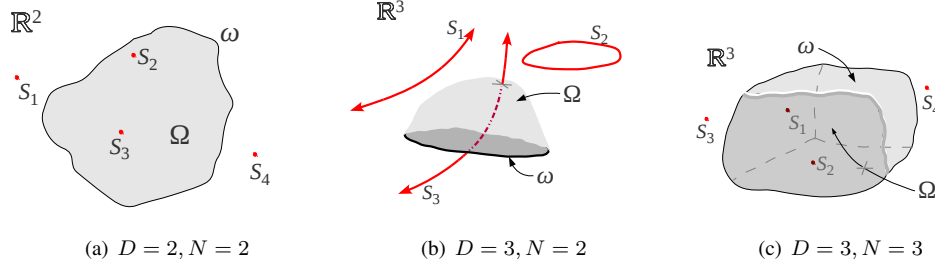


Figure 8: Schematic illustration of some lower dimensional cases of the problem: (a) the Residue theorem, (b) Ampere's law, and (c) Gauss' theorem.

5 Validations in Low Dimensions

In this section we illustrate the forms that equations (11) and (12) take under certain special cases. We compare those with the well-known formulae from complex analysis, electromagnetism and electrostatics that are known to give homology class invariants. Once again, we demonstrate all the computations using a single connected component of \tilde{S} .

5.1 $D = 2, N = 2$:

This particular case has parallels with the *Cauchy integral theorem* and the *Residue theorem* from *Complex analysis*. This formula was used in [3] for designing a H -signature in the 2-dimensional case. Here a singularity manifold, S , is a $D - N = 0$ -dimensional manifold, *i.e.* a point, the coordinate of which we represent by $\mathbf{S} = [s_1, s_2]^T$ (Figure 8(a)).

Thus, the partitions in (12) for the different values of k are as follows,

$$\text{For } k = 1, \text{ part}^0(\{2\}) = \left\{ \{\{\}, \{2\}\} \right\},$$

$$\text{For } k = 2, \text{ part}^0(\{1\}) = \left\{ \{\{\}, \{1\}\} \right\}$$

Thus,

$$U_1^1(\mathbf{x}) = \frac{1}{2\pi} (-1)^{2-2+1+1} (1) \frac{x_1 - S_1}{|\mathbf{x} - \mathbf{S}|^2} = \frac{1}{2\pi} \frac{x_1 - s_1}{|\mathbf{x} - \mathbf{S}|^2}$$

$$U_1^2(\mathbf{x}) = \frac{1}{2\pi} (-1)^{2-2+2+1} (1) \frac{x_2 - S_2}{|\mathbf{x} - \mathbf{S}|^2} = -\frac{1}{2\pi} \frac{x_2 - s_2}{|\mathbf{x} - \mathbf{S}|^2}$$

where the subscripts of U indicate the index of the partition used (in the lists above). Also, note that integration of a 0-form on a 0-dimensional manifold is equivalent to evaluation of the 0-form at the point.

Thus,

$$\begin{aligned} \psi_{\mathbf{S}} &= U_1^1(\mathbf{x})dx_2 + U_1^2(\mathbf{x})dx_1 \\ &= \frac{1}{2\pi} \frac{(x_1 - s_1)dx_2 - (x_2 - s_2)dx_1}{|\mathbf{x} - \mathbf{S}|^2} \\ &= \frac{1}{2\pi} \text{Im} \left(\frac{1}{z - \mathbf{S}_c} dz \right) \end{aligned}$$

where in the last expression we used the complex variables, $z = x_1 + ix_2$ and $\mathbf{S}_c = s_1 + is_2$. In fact, from complex analysis (Residue theorem and Cauchy integral theorem) we know that $\int_{\gamma} \frac{1}{z - \mathbf{S}_c} dz$

(where γ is a closed curve in \mathbb{C}) is $2\pi i$ if γ encloses S_c , but zero otherwise. This is just the fact that

$$\int_{\gamma} \psi_S = \int_{\text{Ins}(\gamma)} d\psi_S = \begin{cases} \pm 1, & \text{if Ins}(\gamma) \text{ contains } S \\ 0, & \text{otherwise} \end{cases}$$

where $\text{Ins}(\gamma)$ represents the inside region of the curve γ , *i.e.* the area enclosed by it.

5.2 $D = 3, N = 2$:

This particular case has parallels with the *Ampere's Law* and the *Biot-Savart Law* from *Electromagnetism*. Here a singularity manifold, S , is a $D - N = 1$ -dimensional manifold, which, in electromagnetics, represents a current-carrying line/wire.

The partitions in (12) for the different values of k are as follows,

$$\text{For } k = 1, \text{ part}^1(\{2, 3\}) = \left\{ \{\{2\}, \{3\}\}, \{\{3\}, \{2\}\} \right\},$$

$$\text{For } k = 2, \text{ part}^1(\{1, 3\}) = \left\{ \{\{1\}, \{3\}\}, \{\{3\}, \{1\}\} \right\},$$

$$\text{For } k = 3, \text{ part}^1(\{1, 2\}) = \left\{ \{\{1\}, \{2\}\}, \{\{2\}, \{1\}\} \right\},$$

Thus,

$$U_1^1(\mathbf{x}) = \frac{1}{4\pi} (-1)^{3-2+1+1} (1) \int_S \frac{x_1 - x'_1}{|\mathbf{x} - \mathbf{x}'|^3} dx'_2 = -\frac{1}{4\pi} \int_S \frac{x_1 - x'_1}{|\mathbf{x} - \mathbf{x}'|^3} dx'_2$$

$$U_2^1(\mathbf{x}) = \frac{1}{4\pi} (-1)^{3-2+1+1} (-1) \int_S \frac{x_1 - x'_1}{|\mathbf{x} - \mathbf{x}'|^3} dx'_3 = \frac{1}{4\pi} \int_S \frac{x_1 - x'_1}{|\mathbf{x} - \mathbf{x}'|^3} dx'_3$$

$$U_1^2(\mathbf{x}) = \frac{1}{4\pi} (-1)^{3-2+2+1} (1) \int_S \frac{x_2 - x'_2}{|\mathbf{x} - \mathbf{x}'|^3} dx'_1 = \frac{1}{4\pi} \int_S \frac{x_2 - x'_2}{|\mathbf{x} - \mathbf{x}'|^3} dx'_1$$

$$U_2^2(\mathbf{x}) = \frac{1}{4\pi} (-1)^{3-2+2+1} (-1) \int_S \frac{x_2 - x'_2}{|\mathbf{x} - \mathbf{x}'|^3} dx'_3 = -\frac{1}{4\pi} \int_S \frac{x_2 - x'_2}{|\mathbf{x} - \mathbf{x}'|^3} dx'_3$$

$$U_1^3(\mathbf{x}) = \frac{1}{4\pi} (-1)^{3-2+3+1} (1) \int_S \frac{x_3 - x'_3}{|\mathbf{x} - \mathbf{x}'|^3} dx'_1 = -\frac{1}{4\pi} \int_S \frac{x_3 - x'_3}{|\mathbf{x} - \mathbf{x}'|^3} dx'_1$$

$$U_2^3(\mathbf{x}) = \frac{1}{4\pi} (-1)^{3-2+3+1} (-1) \int_S \frac{x_3 - x'_3}{|\mathbf{x} - \mathbf{x}'|^3} dx'_2 = \frac{1}{4\pi} \int_S \frac{x_3 - x'_3}{|\mathbf{x} - \mathbf{x}'|^3} dx'_2$$

where, as before, the subscripts of U indicate the index of the partition used (in the lists above).

Thus,

$$\begin{aligned} \psi_S &= U_1^1(\mathbf{x})dx_3 + U_2^1(\mathbf{x})dx_2 + U_1^2(\mathbf{x})dx_3 + U_2^2(\mathbf{x})dx_1 + U_1^3(\mathbf{x})dx_2 + U_2^3(\mathbf{x})dx_1 \\ &= (U_2^2(\mathbf{x}) + U_2^3(\mathbf{x}))dx_1 + (U_2^1(\mathbf{x}) + U_1^3(\mathbf{x}))dx_2 + (U_1^1(\mathbf{x}) + U_1^2(\mathbf{x}))dx_3 \\ &= \begin{bmatrix} U_2^2(\mathbf{x}) + U_2^3(\mathbf{x}) \\ U_2^1(\mathbf{x}) + U_1^3(\mathbf{x}) \\ U_1^1(\mathbf{x}) + U_1^2(\mathbf{x}) \end{bmatrix} \cdot \wedge \begin{bmatrix} dx_1 \\ dx_2 \\ dx_3 \end{bmatrix} \\ &= \frac{1}{4\pi} \int_S \begin{bmatrix} -\frac{x_2 - x'_2}{|\mathbf{x} - \mathbf{x}'|^3} dx'_3 + \frac{x_3 - x'_3}{|\mathbf{x} - \mathbf{x}'|^3} dx'_2 \\ \frac{x_1 - x'_1}{|\mathbf{x} - \mathbf{x}'|^3} dx'_3 - \frac{x_3 - x'_3}{|\mathbf{x} - \mathbf{x}'|^3} dx'_1 \\ -\frac{x_1 - x'_1}{|\mathbf{x} - \mathbf{x}'|^3} dx'_2 + \frac{x_2 - x'_2}{|\mathbf{x} - \mathbf{x}'|^3} dx'_1 \end{bmatrix} \cdot \wedge \begin{bmatrix} dx_1 \\ dx_2 \\ dx_3 \end{bmatrix} \\ &= \frac{1}{4\pi} \int_S \frac{d\mathbf{l}' \times (\mathbf{x} - \mathbf{x}')}{|\mathbf{x} - \mathbf{x}'|^3} \cdot \wedge \begin{bmatrix} dx_1 \\ dx_2 \\ dx_3 \end{bmatrix} \end{aligned}$$

where, bold face indicates column 3-vectors and the cross product “ \times ”: $\mathbb{R}^3 \times \mathbb{R}^3 \rightarrow \mathbb{R}^3$ is the elementary cross product operation of column 3-vectors. The operation “ $\cdot \wedge$ ” between column vectors implies element-wise wedge product followed by summation. Also, $d\mathbf{l}' = [dx'_1 \ dx'_2 \ dx'_3]^T$. It is not difficult to identify the integral in the last expression, $\mathbf{B} = \frac{1}{4\pi} \int_S \frac{d\mathbf{l}' \times (\mathbf{x} - \mathbf{x}')}{|\mathbf{x} - \mathbf{x}'|^3}$ with the *Magnetic Field vector* created by unit current flowing through S , computed using the *BiotSavart law*. Thus, if γ is a closed loop, the statement of the *Ampere's circuital law* gives, $\int_\gamma \mathbf{B} \cdot d\mathbf{l} = \int_\gamma \psi_S = I_{encl}$, the current encloses by the loop.

5.3 $D = 3, N = 3$:

This particular case has parallels with the *Gauss's law* in *Electrostatics*, and in general the *Gauss Divergence theorem*. Here a singularity manifold, S , is a $D - N = 0$ -dimensional manifold, i.e. a point, the coordinate of which is represented by $\mathbf{S} = [S_1, S_2, S_3]^T$, which in the light of *Electrostatics*, is a point charge. The candidate manifolds are 2-dimensional surfaces (Figure 8(c)).

The partitions in (12) for the different values of k are as follows,

$$\begin{aligned} \text{For } k = 1, \quad part^0(\{2, 3\}) &= \left\{ \{\{\}, \{2, 3\}\} \right\}, \\ \text{For } k = 2, \quad part^0(\{1, 3\}) &= \left\{ \{\{\}, \{1, 3\}\} \right\}, \\ \text{For } k = 3, \quad part^0(\{1, 2\}) &= \left\{ \{\{\}, \{1, 2\}\} \right\}, \end{aligned}$$

Here, $D - N = 0$ implies the integration of (11) once again becomes evaluation of 0-forms at \mathbf{S} . Thus,

$$\begin{aligned} U_1^1(\mathbf{x}) &= \frac{1}{4\pi} (-1)^{3-3+1+1} (1) \frac{x_1 - S_1}{|\mathbf{x} - \mathbf{S}|^3} = \frac{1}{4\pi} \frac{x_1 - S_1}{|\mathbf{x} - \mathbf{S}|^3} \\ U_1^2(\mathbf{x}) &= \frac{1}{4\pi} (-1)^{3-3+2+1} (1) \frac{x_2 - S_2}{|\mathbf{x} - \mathbf{S}|^3} = -\frac{1}{4\pi} \frac{x_2 - S_2}{|\mathbf{x} - \mathbf{S}|^3} \\ U_1^3(\mathbf{x}) &= \frac{1}{4\pi} (-1)^{3-3+3+1} (1) \frac{x_3 - S_3}{|\mathbf{x} - \mathbf{S}|^3} = \frac{1}{4\pi} \frac{x_3 - S_3}{|\mathbf{x} - \mathbf{S}|^3} \end{aligned}$$

Thus,

$$\begin{aligned} \psi_S &= U_1^1(\mathbf{x}) dx_2 \wedge dx_3 + U_1^2(\mathbf{x}) dx_1 \wedge dx_3 + U_1^3(\mathbf{x}) dx_1 \wedge dx_2 \\ &= \frac{1}{4\pi} \left(\frac{x_1 - S_1}{|\mathbf{x} - \mathbf{S}|^3} dx_2 \wedge dx_3 + \frac{x_2 - S_2}{|\mathbf{x} - \mathbf{S}|^3} dx_3 \wedge dx_1 + \frac{x_3 - S_3}{|\mathbf{x} - \mathbf{S}|^3} dx_1 \wedge dx_2 + \right) \\ &= \left(\frac{1}{4\pi} \frac{\mathbf{x} - \mathbf{S}}{|\mathbf{x} - \mathbf{S}|^3} \right) \cdot \wedge [dx_2 \wedge dx_3, dx_3 \wedge dx_1, dx_1 \wedge dx_2]^T \end{aligned} \quad (16)$$

The quantity $\mathbf{E} = \frac{1}{4\pi} \frac{\mathbf{x} - \mathbf{S}}{|\mathbf{x} - \mathbf{S}|^3}$ can be readily identified with the electric field created by an unit point charge at \mathbf{S} . If \mathcal{A} is a closed surface, then $\int_{\mathcal{A}} \mathbf{E} \cdot d\mathbf{A} = \int_{\mathcal{A}} \psi_S = Q_{encl}$, the charge enclosed by \mathcal{A} .

6 Examples and Applications

We implemented the general formula for computing $\psi_S(\omega)$ in C++ for arbitrary D and N . The singularity manifolds, S , and the candidate manifold, ω , are discretized to create simplicial complexes \bar{S} and $\bar{\omega}$ respectively, thus enabling us to compute the integral in equations (10) and (11) as a sum of integrals over simplices. In the following section, for simplicity, we use the same notation for the manifolds and their simplicial equivalents. We used the *Armadillo linear programming library*

[15] for all vector and matrix operations, and the *GNU Scientific Library* [10] for all the numerical integrations.

6.1 An Example for $D = 5, N = 3$

In Section 5 we have shown that the general formulation we proposed in Section 4 indeed reduces to known formulae that gives us the homology class invariants for certain low dimensional cases. We present numerical validation for a simple case of dimension greater than three: $D = 5$ and $N = 3$. The candidate manifold is of dimension $N - 1 = 2$. We consider a 2-sphere centered at the origin in \mathbb{R}^5 as the candidate manifold: let $\omega(R_C) = \{\mathbf{x} \mid x_1^2 + x_2^2 + x_3^2 = R_C^2, x_4 = 0, x_5 = 0\}$ be the boundary of the ball $\Omega(R_C) = \{\mathbf{x} \mid x_1^2 + x_2^2 + x_3^2 \leq R_C^2, x_4 = 0, x_5 = 0\}$. The candidate manifold $\omega(R_C)$ is easily parametrized via spherical coordinates θ and ϕ .

$$\begin{aligned} x_1 &= R_C \cos(\theta) \cos(\phi) \\ x_2 &= R_C \cos(\theta) \sin(\phi) \\ x_3 &= R_C \sin(\theta) \\ x_4 &= 0 \\ x_5 &= 0 \end{aligned} \tag{17}$$

Let the singularity manifold S be the 2-torus as follows:

$$\begin{aligned} x_1 &= 0 \\ x_2 &= 0 \\ x_3 &= (R_T + r \cos(\phi')) \cos(\theta') - (R_T + r) \\ x_4 &= (R_T + r \cos(\phi')) \sin(\theta') \\ x_5 &= r \sin(\phi) \end{aligned} \tag{18}$$

with $R_T > r$ and the parameters $\theta' \in [0, 2\pi]$ and $\phi' \in [0, 2\pi]$. For all examples that follow, we choose $r = 0.8, R_T = 1.6$.

Consider the particular candidate manifold $\omega(1)$ (*i.e.* $R_C = 1$). By numerical computation of integrals in (10) and (11), the value of $\phi_S(\omega(1))$ that we obtain for the above example is -1 . In order to interpret this result we first observe that $\omega(1)$ does not intersect S (*i.e.* there is no common solution for (17) and (18) with $R_C = 1.0, r = 0.8, R_T = 1.6$). However on S , when $x_1 = x_2 = x_4 = x_5 = 0$, x_3 can assume the values $0, -2r, -2R_T$ and $-2(R_T + r)$. Thus, if $2r > R_C$, S intersects $\Omega(R_C)$ (the ball whose boundary is $\omega(R_C)$) only at one point, the origin. A simple computation of the tangents reveals that the intersection is transverse. Since that is a single transverse intersection with $\Omega(R_C)$, the linking number between $\omega(R_C)$ and S (*i.e.* intersection number between $\Omega(R_C)$ and S according to Definition D2) is ± 1 for all $R_C < 2r$, just as indicated by the value of $\phi_S(\omega(1))$. The sign is not of importance since that is determined by our choice of orientation. In fact, with different values of R_C, r and R_T , as long as $R_T > r > \frac{R_C}{2}$, we obtain the same value of -1 for $\phi_S(\omega(R_C))$.

However with $R_C = 2$ for the candidate manifold, and the singularity manifold remaining the same (*i.e.* $r = 0.8, R_T = 1.6$), the value of $\phi_S(\omega(2))$ we obtain numerically is 0. In this case, the points at which S intersect $\Omega(2)$ are the origin and the point $(x_1 = x_2 = x_4 = x_5 = 0, x_3 = -0.8)$. Of course, in the family of candidate manifolds $\omega(R_C)$, $R_C \in [1, 2]$, we can easily observe that $\omega(1.6)$ indeed intersects S , thus indicating that $\omega(1)$ and $\omega(2)$ are possibly in different homology classes.

Next, consider the following family of candidate manifolds:

$$\omega'(T_C) = \{\mathbf{x} \mid x_1^2 + x_2^2 + x_3^2 = 2.0, x_4 = 0, x_5 = T_C\} \tag{19}$$

and a corresponding $\Omega'(T_C)$ such that $\omega'(T_C) = \partial\Omega'(T_C)$:

$$\Omega'(T_C) = \{\mathbf{x} \mid x_1^2 + x_2^2 + x_3^2 \leq 2, x_4 = 0, x_5 = T_C\} \quad (20)$$

With the same S as before, if $T_C > r$, clearly there is no intersection between $\Omega'(T_C)$ and S . Thus it is not surprising that indeed by numerical computation, we found that $\phi_S(\omega'(1)) = 0$.

Now, since we computed $\phi_S(\omega(2)) = 0$ (although $\Omega(2)$ intersects S at 2 points) and $\phi_S(\omega'(1)) = 0$ (and $\Omega'(1)$ does not intersect S), it suggests that $\omega(2)$ and $\omega'(1)$ are in the same homology class. We verify this by observation. None from the family of candidate manifolds $\omega'(T_C)$, $\forall T_C \in [0, 1]$ intersect S , and each is a 2-sphere. Thus ω' defines an embedding of $\mathbb{S}^2 \times I$ in $\mathbb{R}^5 - S$ such that $\omega'(0) \sqcup -\omega'(1)$ is its boundary. It follows that $\omega'(0)$ and $\omega'(1)$ are homologous. However, $\omega(2) = \omega'(0)$. Thus it follows that $\omega(2)$ and $\omega'(1)$ are homologous.

6.2 Application to Graph Search-based Robot Path Planning with Topological Constraints

One consequence of $\phi_{\tilde{S}}$ being a cocycle is that it is a linear function. As a result, if we have a cycle $\bar{\omega}$ that can be expressed as a sum of chains, *i.e.* $\bar{\omega} = \sum_i \bar{\tau}_i$, with $\bar{\tau}_i \in C_{N-1}(\mathbb{R}^D - \tilde{S})$, then we can write

$$\phi_{\tilde{S}}(\bar{\omega}) = \sum_i \phi_{\tilde{S}}(\bar{\tau}_i) \quad (21)$$

where by $\phi_{\tilde{S}}(\bar{\tau}_i)$ we simply mean the vector formed by evaluation of the integrals in Equations (15).

Remark 1. Given $(N-1)$ -chains, $\bar{\tau}_1$ and $\bar{\tau}_2$ in X , such that $\partial\bar{\tau}_1 = \partial\bar{\tau}_2$, by an abuse of terminology in the following discussions, we will say that they are in the same homology class if $\bar{\tau}_1 - \bar{\tau}_2$ is null-homologous in X . It should however be remembered that homology classes are not formally defined for chains, and are defined only for cycles or relative cycles.

That is, in the context of our problem where $X = (\mathbb{R}^D - \tilde{\mathcal{O}})$, $\bar{\tau}_1 \approx \bar{\tau}_2$ iff $\phi_{\tilde{S}}(\bar{\tau}_1 - \bar{\tau}_2) = 0$ (where \tilde{S} is the equivalent of $\tilde{\mathcal{O}}$ satisfying the property of Proposition P1). In context of robot path planning problem, the candidate manifolds are all 1-dimensional. Thus we have $N = 2$. While trajectories connecting two points in a configuration space $(\mathbb{R}^D - \tilde{\mathcal{O}})$ themselves are not closed manifolds, two trajectories connecting the same points together form a closed manifold.

Next we outline the basic graph construction for search-based planning with topological constraints (*cf.* the H -augmented graph of [3]). Discrete graph search techniques for robot path planning problems are widely used and have been shown to be complete and efficient [17, 8]. Given a D -dimensional configuration space, the standard starting point is to discretize the configuration space, place vertices inside each discrete cell, and establish edges between the neighboring vertices to create a directed graph, $\mathcal{G} = (\mathcal{V}, \mathcal{E})$ (Figure 9(a)). The discretization itself can be quite arbitrary and non-uniform in general. A directed edge $[\mathbf{v}_1, \mathbf{v}_2] \in \mathcal{E}$ connects vertices \mathbf{v}_1 to \mathbf{v}_2 iff there is a single action of the robot that can take it from state \mathbf{v}_1 to state \mathbf{v}_2 . Since an edge $[\mathbf{v}_1, \mathbf{v}_2] \in \mathcal{E}$ is a 1-dimensional manifold embedded in $(\mathbb{R}^D - \tilde{S})$, we can evaluate the function $\phi_{\tilde{S}}$ on (a top-dimensional covering chain on) it and write it as $\phi_{\tilde{S}}([\mathbf{v}_1, \mathbf{v}_2])$. Likewise, a path, λ , in the graph (Figure 9(b)) can be represented by a covering chain $\bar{\lambda} \in H_{N-1}(\mathbb{R}^D - \tilde{S})$, and $\phi_{\tilde{S}}$ can be evaluated on it. For simplicity, we often write $\phi_{\tilde{S}}(\lambda)$ to indicate this quantity, which is made possible due to the assumption that such covering chains are essentially constructed out of simplices with unit coefficients. The weight/cost of each edge is the cost of traversing that edge by the robot (typically the metric length of the edge). We write $w([\mathbf{v}_1, \mathbf{v}_2])$ to represent the weight of an edge. Inaccessible

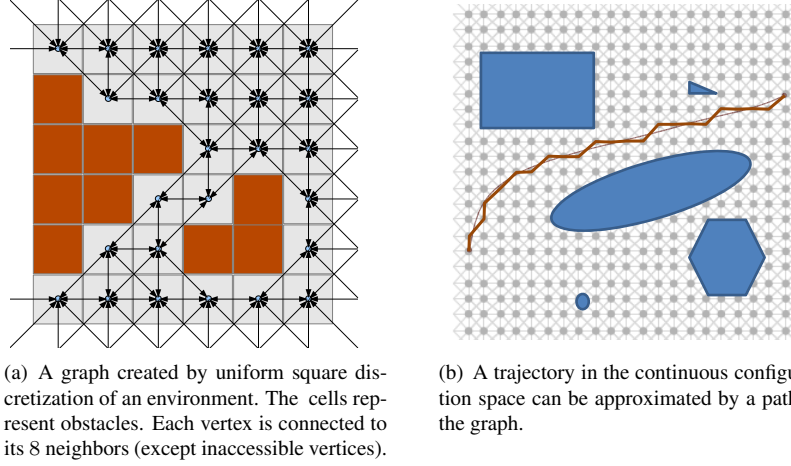


Figure 9: Graph, \mathcal{G} , created by uniform discretization of an environment. This specific type of graph shown in the figures is referred to as the 8-connected grid.

coordinates (lying inside obstacles or outside a specified workspace) do not constitute nodes of the graph. A path in this graph represents a trajectory of the robot in the configuration space. The triangulation of any path in the graph essentially consists of the directed edges of the graph that make up the path.

Suppose we are given a fixed start and a fixed goal coordinate, represented by $\mathbf{v}_s, \mathbf{v}_g \in (\mathbb{R}^D - \tilde{\mathcal{O}})$ respectively, for the robot (by the boldface \mathbf{v} 's, with a slight abuse of notation, we will indicate both the vertex in the graph as well as the coordinate of the vertex in the original configuration space). We next construct an augmented graph, $\hat{\mathcal{G}} = \{\hat{\mathcal{V}}, \hat{\mathcal{E}}\}$, from the graph \mathcal{G} in order to incorporate the information regarding the homology class of trajectories leading from the given start coordinate to the goal coordinate, as follows.

1.

$$\hat{\mathcal{V}} = \left\{ \{\mathbf{v}, \mathbf{c}\} \left| \begin{array}{l} \mathbf{v} \in \mathcal{V}, \text{ and,} \\ \mathbf{c} \text{ is a } m\text{-vector of reals such that } \mathbf{c} = \phi_{\hat{\mathcal{S}}}(\bar{\lambda}) \\ \text{for some 1-chain, } \bar{\lambda}, \text{ with boundary } \mathbf{v}_s \sqcup -\mathbf{v} \\ \text{(i.e. } \bar{\lambda} \text{ is a covering chain of some path in } \mathcal{G} \text{ connecting } \mathbf{v}_s \text{ to } \mathbf{v}). \end{array} \right. \right\}$$

2. An edge $[\{\mathbf{v}, \mathbf{c}\}, \{\mathbf{v}', \mathbf{c}'\}]$ exists in $\hat{\mathcal{E}}$ for $[\mathbf{v}, \mathbf{c}] \in \hat{\mathcal{V}}$ and $[\mathbf{v}', \mathbf{c}'] \in \hat{\mathcal{V}}$, iff

- i. The edge $[\mathbf{v}, \mathbf{v}'] \in \mathcal{E}$, and,
- ii. $\mathbf{c}' = \mathbf{c} + \phi_{\hat{\mathcal{S}}}([\mathbf{v}, \mathbf{v}'])$.

3. The cost/weight associated with an edge $[\{\mathbf{v}, \mathbf{c}\}, \{\mathbf{v}', \mathbf{c}'\}]$ is same as the cost/weight associated with edge $[\mathbf{v}, \mathbf{v}'] \in \mathcal{E}$. That is, the weight function we use is $\hat{w}([\{\mathbf{v}, \mathbf{c}\}, \{\mathbf{v}', \mathbf{c}'\}]) = w([\mathbf{v}, \mathbf{v}'])$.

It can be noted that $\{\mathbf{v}_s, \mathbf{0}\}$ is in $\hat{\mathcal{V}}$ (where $\mathbf{0}$ is an m -vector of zeros).

For finding a least cost path in $\hat{\mathcal{G}}$ that belongs to a particular homotopy class, we can use a heuristic graph search algorithm (e.g. weighted A*) [12, 6, 14]. In particular, we used the YAGSBPL

library [2] for constructing the graph and performing A* searches in it. Starting from the start vertex $\{\mathbf{v}_s, \mathbf{0}\}$ we expand the vertices in $\hat{\mathcal{G}}$. The process of vertex expansion eventually leads to vertices of the form $\{\mathbf{v}_g, \mathbf{c}_i\}$, where $\mathbf{c}_i = \phi_{\tilde{\mathcal{S}}}(\lambda_{sg})$ for some path λ_{sg} in \mathcal{G} connecting \mathbf{v}_s to \mathbf{v}_g . Each of these vertices in $\hat{\mathcal{G}}$ correspond to an unique homology class of the path taken to reach \mathbf{v}_g from \mathbf{v}_s . Let those vertices in the order in which we expand them be $\{\mathbf{v}_g, \mathbf{c}_1\}$, $\{\mathbf{v}_g, \mathbf{c}_2\}$, etc. Say during the search process, we expand the vertex $\{\mathbf{v}_g, \mathbf{c}_j\} \in \hat{\mathcal{V}}$. Depending on whether we are trying to search for a particular homology class of trajectories or exploring multiple homology classes, we can choose to take one of the following actions:

- i. If \mathbf{c}_j is the desired value (or an admitted value) for the $\phi_{\tilde{\mathcal{S}}}$ -value of the trajectory we are searching for, we store the path up to $\{\mathbf{v}_g, \mathbf{c}_j\}$ in $\hat{\mathcal{G}}$, and stop the search algorithm.
- ii. If \mathbf{c}_j is an admitted value for the $\phi_{\tilde{\mathcal{S}}}$ -value of the trajectory we are searching for, we store the path up to $\{\mathbf{v}_g, \mathbf{c}_j\}$ in $\hat{\mathcal{G}}$, and continue expanding vertices in $\hat{\mathcal{G}}$.
- iii. If \mathbf{c}_j is not an admitted value for the $\phi_{\tilde{\mathcal{S}}}$ -value of the trajectory we are searching for, we continue expanding vertices in $\hat{\mathcal{G}}$.

Clearly, the projection of any of the stored trajectories onto \mathcal{G} are paths in \mathcal{G} connecting \mathbf{v}_s to \mathbf{v}_g . Since both $\hat{\mathcal{G}}$ and \mathcal{G} use the same cost function, if $\{\{\mathbf{v}_s, \mathbf{0}\}, \{\mathbf{v}^{1*}, \mathbf{c}^{1*}\}, \{\mathbf{v}^{2*}, \mathbf{c}^{2*}\}, \dots, \{\mathbf{v}_g, \mathbf{c}_j\}\}$ is the j^{th} stored path using an optimal search algorithm (e.g. A*), then $\{\mathbf{v}_s, \mathbf{v}^{1*}, \mathbf{v}^{2*}, \dots, \mathbf{v}_g\}$ is the optimal path in \mathcal{G} with $\phi_{\tilde{\mathcal{S}}}$ -value of \mathbf{c}_j (i.e. least cost path belonging to the particular homology class). Thus we can explore the different homology classes of the trajectories connecting \mathbf{v}_s to \mathbf{v}_g .

If \mathbf{c}_g is the desired value of $\phi_{\tilde{\mathcal{S}}}$ evaluated on the trajectory we are searching for, we follow the above process of expanding the vertices using the graph search algorithm until we expand $\{\mathbf{v}_g, \mathbf{c}_g\}$. Given two paths λ_1, λ_2 in \mathcal{G} , and if $\bar{\lambda}_1, \bar{\lambda}_2$ are their respective covering chains, since $\bar{\lambda}_1 \sqcup -\bar{\lambda}_2 \in C_{N-1}(\mathbb{R}^D - \tilde{\mathcal{S}})$, we notice that $(\phi_{\tilde{\mathcal{S}}}(\bar{\lambda}_1) - \phi_{\tilde{\mathcal{S}}}(\bar{\lambda}_2)) \in \mathbb{Z}^m$ (with unit coefficients on the simplices that constitute the chains, and with the choice of $\phi_{\tilde{\mathcal{S}}}$ as described in Equations (10) and (15)). Thus, if we know the value of a $\mathbf{c}_j = \chi_{\tilde{\mathcal{S}}}(\bar{\lambda}_j)$, we can construct another m -vector that is a valid value for $\phi_{\tilde{\mathcal{S}}}$ evaluated on some other trajectory connecting \mathbf{v}_s to \mathbf{v}_g as $\mathbf{c}_{j'} = \mathbf{c}_j + \zeta$ for some $\zeta \in \mathbb{Z}^m$. This we can hence set as \mathbf{c}_g for finding the least cost path in the new homology class.

A consequence of the point 3 in the definition of \mathcal{G}_χ is that any *admissible heuristics* (which is a lower bound on the cost to the goal vertex) in \mathcal{G} will remain admissible in $\hat{\mathcal{G}}$. That is, if $h(\mathbf{v}, \mathbf{v}')$ was the heuristic function in \mathcal{G} , we can define $\hat{h}(\{\mathbf{v}, \mathbf{c}\}, \{\mathbf{v}', \mathbf{c}'\}) = h(\mathbf{v}, \mathbf{v}')$ as the heuristic function in $\hat{\mathcal{G}}$. As a consequence, if we keep expanding vertices in $\hat{\mathcal{G}}$ as described in the previous section, the order in which we will encounter states of the form $\{\mathbf{v}_g, \mathbf{c}_i\}$ is the order of the costs of the least cost paths in the different homology classes.

6.2.1 Planning in Low Dimensional Configuration Spaces

Figure 10 shows a 2-dimensional region punctured by two obstacles. The graph \mathcal{G} is constructed by uniform square discretization (200×200), placing a vertex in each cell, and by connecting the free/accessible neighboring vertices (Figure 9(a)). During the search of graph $\hat{\mathcal{G}}$, we adopt the action ‘ii.’ whenever we encounter a vertex of the form $\{\mathbf{v}_g, \mathbf{c}_j\} \in \hat{\mathcal{V}}$, until we have stored 10 paths. One can choose the *bump 1-form* [4] for constructing $\psi_{\tilde{\mathcal{S}}}$ as discussed earlier. The *supports* of that form are illustrated in the figure as the thin rays.

Figure 11 demonstrates an example of search for 3 homology classes in a configuration space with $D = 3$. The graph \mathcal{G} is created by uniform discretization of the region of interest into $16 \times$

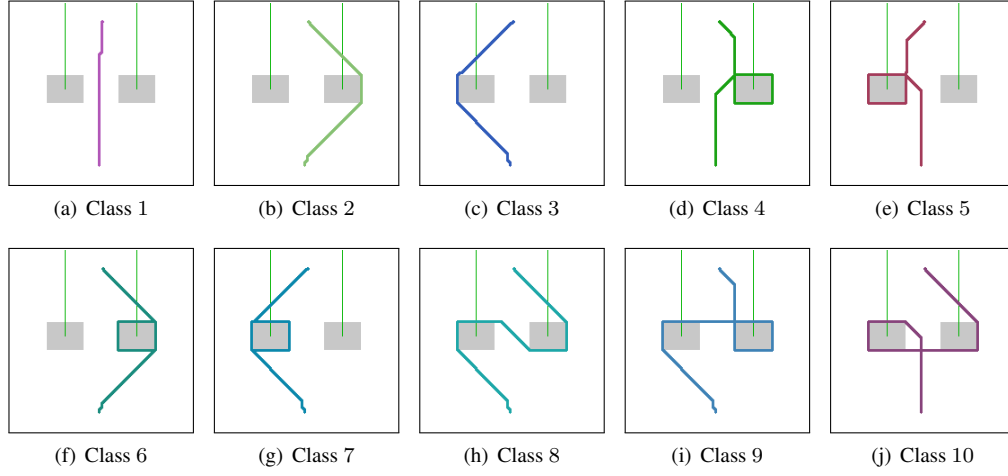


Figure 10: The first 10 homology classes of trajectories in order of length/cost. The gray regions are the obstacles. The trajectories are in different homotopy classes as well.

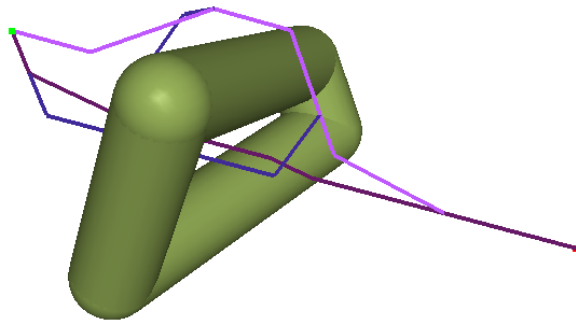


Figure 11: Exploration of 3 homology classes of robot trajectories for a $D = 3$ -dimensional configuration space.

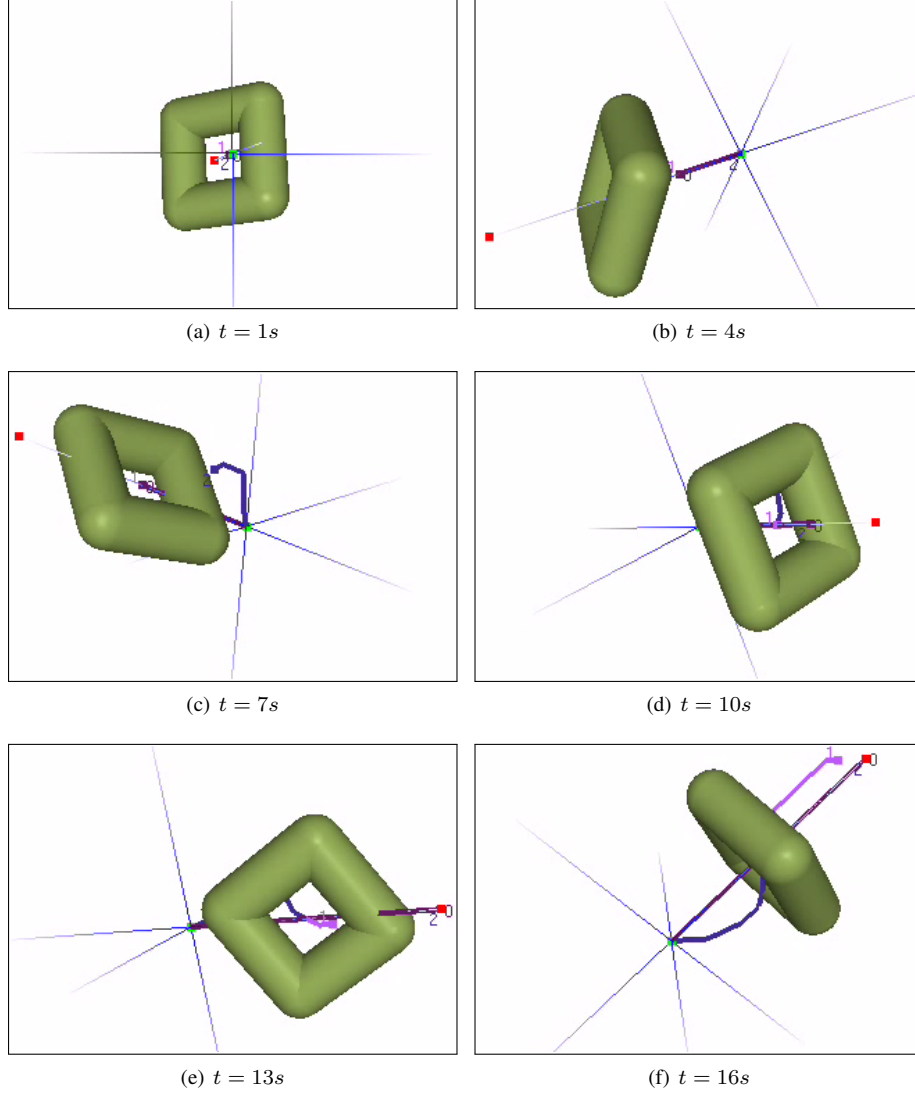


Figure 12: Screenshots from exploration of 3 homotopy classes in a $X - Y - Z - Time$ configuration space. The loop-shaped obstacle is rotating about an axis. The X , Y and Z axes are shown. Their apparent rotation is due to movement of the *camera* for viewing from different angles.

16×16 cubic cells, and connecting the vertices corresponding to each cell to their immediate 26 neighbors.

6.2.2 Exploring Paths in Different Homotopy Classes in a 4-dimensional Space

Just as we developed formulae for complete invariants for homology class in the 2 and 3 dimensional cases in [3], we can now extend the formula to trajectories in higher dimensional spaces using the

invariant described in Equation (15).

In this example we explore homology classes of trajectories in a 3-dimensional space with moving obstacles. However that makes the configuration space a 4-dimensional one consisting of the coordinates X, Y, Z and $Time$. Thus we present a result in a $X - Y - Z - Time$ configuration space where we find multiple shortest paths in different homology classes in the 4-dimensional space. Figure 12 shows the exploration of 3 homology classes in a 4-dimensional configuration space consisting of a dynamic obstacle in 3-dimensions. The loop-shaped obstacle is rotating about an axis. The X, Y and Z axes are shown. As we observe in the sequence, trajectories numbered 0 and 1 take off from the start coordinate (green dot) and move towards the “center” of the loop. They wait there while 2 takes a different homotopy class to reach the center later. From there 0 and 2 head together towards the goal (red dot), while 1 wait to take a different trajectory to the goal. Thus the 3 trajectories are in different homotopy classes.

7 Extension to non-Euclidean Ambient Spaces

Let L be a subspace of $(\mathbb{R}^D - \tilde{S})$. In this section we would like to compute complete invariants for homology classes of $(N - 1)$ -cycles in the quotient space $(\mathbb{R}^D - \tilde{S})/L$.

We write the inclusion map as $\iota : L \hookrightarrow (\mathbb{R}^D - \tilde{S})$. We consider $(N - 1)$ -chains in $C_{N-1}(\mathbb{R}^D - \tilde{S})$, and their images under the quotient map $q_{\#} : C_{\bullet}(\mathbb{R}^D - \tilde{S}) \rightarrow C_{\bullet}(\mathbb{R}^D - \tilde{S})/C_{\bullet}(L)$. In the following proposition we consider the general pair of spaces (X, L) , and for generality we state it for n -chains.

Let us consider a $(N - 1)$ -chain, $\bar{\alpha} \in C_{N-1}(\mathbb{R}^D - \tilde{S})$ such that its boundary lies completely in L . Let us represent this boundary by $\bar{\beta} \in C_{N-2}(L)$. This is, in general, extremely difficult to achieve. However we will consider a special condition on the relative cycles

Proposition P6. *Let (X, L) be a pair of spaces, $\iota : L \hookrightarrow X$ be the inclusion map, and $q_{\#} : C_{\bullet}(X) \rightarrow C_{\bullet}(X)/C_{\bullet}(L)$ the quotient map for chains. Consider $\bar{\alpha} \in C_n(X)$ such that its boundary, $\partial\bar{\alpha}$, is either empty or lies completely in L . Thus, $q_{\#}(\bar{\alpha})$ is a relative n -cycle in (X, L) . Then, $[q_{\#}(\bar{\alpha})] = 0 \in H_n(X, L)$ if and only if there exists some $\bar{\beta} \in C_n(L)$ with $\iota \circ \partial\bar{\beta} = \partial\bar{\alpha}$, such that $[\bar{\alpha} - \iota \circ \bar{\beta}] = 0 \in H_n(X)$ (see Figure 13(a)).*

Proof.

Suppose there exists $\bar{\beta} \in C_{N-1}(L)$ such that $[\bar{\alpha} - \iota \circ \bar{\beta}] = 0$. Using the homomorphism $q_{\#}$ induced by $q_{\#}$, and noting that $q_{\#}(\iota\bar{\beta}) = 0$, we have from functoriality of homology $q_{\#}([\bar{\alpha} - \iota \circ \bar{\beta}]) = [q_{\#}(\bar{\alpha})] - [q_{\#}(\iota\bar{\beta})] = [q_{\#}(\bar{\alpha})]$. Thus, $[q_{\#}(\bar{\alpha})] = 0$, concluding the “if” part of the proof.

Next, assume $[q_{\#}(\bar{\alpha})] = 0$. Consider the following diagram with exact rows,

$$\begin{array}{ccccccccc} 0 & \longrightarrow & C_{n+1}(L) & \xrightarrow{\iota} & C_{n+1}(X) & \xrightarrow{q_{\#}} & C_{n+1}(X, L) & \longrightarrow & 0 \\ & & \downarrow \tilde{\partial} & & \downarrow \partial & & \downarrow \hat{\partial} & & \\ 0 & \longrightarrow & C_n(L) & \xrightarrow{\iota} & C_n(X) & \xrightarrow{q_{\#}} & C_n(X, L) & \longrightarrow & 0 \end{array} \quad (22)$$

The proof follows from the above diagram using the following sequence of arguments:

$[q_{\#}(\bar{\alpha})] = 0$ implies $q_{\#}(\bar{\alpha}) \in C_n(X, L)$ is a relative boundary. Thus, there exists some $\bar{\gamma} \in C_{n+1}(X, L)$ such that $q_{\#}(\bar{\alpha}) = \hat{\partial}\bar{\gamma}$. Due to surjectivity of $q_{\#}$ (since the rows are exact), then there exists a $\bar{A} \in C_{n+1}(X)$ such that $q_{\#}(\bar{A}) = \bar{\gamma}$. Hence, from the commutativity of the right square, we have $q_{\#} \circ \partial(\bar{A}) = \hat{\partial} \circ q_{\#}(\bar{A}) = \hat{\partial}\bar{\gamma} = q_{\#}(\bar{\alpha})$. Hence, $q_{\#}(\bar{\alpha} - \partial\bar{A}) = 0 \in C_n(X, L)$. Thus, $(\bar{\alpha} - \partial\bar{A}) \in \text{Ker}(q_{\#}) \subseteq C_n(X)$. Finally, using the exactness of the second row, there should hence exist a $\bar{\beta} \in C_n(L)$ such that $\iota(\bar{\beta}) = \bar{\alpha} - \partial\bar{A}$. Thus, $\bar{\alpha} - \iota(\bar{\beta}) = \partial\bar{A}$, which is a n -boundary. Hence proved.

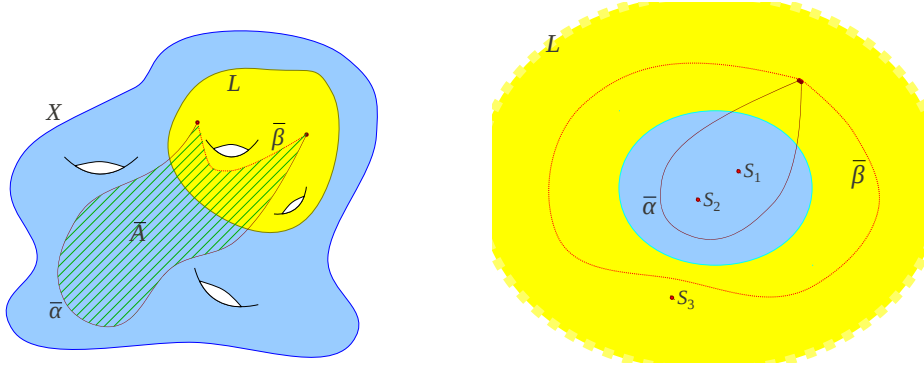


Figure 13: (left) An illustration of a relative cycle. (right). An example with $X = \mathbb{R}^2 - (S_1 \sqcup S_2 \sqcup S_3)$, $N = 2$. The region, L , consists of everything that lies outside the small disk-shaped region, moding which out gives us the 2-sphere with two punctures (images of S_1 and S_2). $\bar{\alpha}$ is a non-trivial cycle in $\mathbb{R}^2 - (S_1 \sqcup S_2 \sqcup S_3)$ since $\phi_{\bar{S}}(\bar{\alpha}) = [1, 1, 0]$. However it is trivial on the punctured sphere. To see this, we observe that in this case $Q = \{[0, 0, 0], [\pm 1, \pm 1, 0], [\pm 2, \pm 2, 0], \dots, [0, 0, 1], [\pm 1, \pm 1, 1], \dots, [0, 0, 2], \dots, \dots\}$. Thus we see that $\phi_{\bar{S}}(\bar{\alpha}) \in Q$. A $\bar{\beta} \in C_{N-1}(L)$ corresponding to the class is shown in the figure.

For simplicity, the following diagram illustrates the quantities introduced in the above argument:

$$\begin{array}{ccccc}
 \bar{A} & & \xrightarrow{q_{\#}} & \bar{\gamma} & \longrightarrow 0 \\
 \downarrow \partial & & & \downarrow \hat{\partial} & \\
 \bar{\alpha}, \partial \bar{A} & & \xrightarrow{q_{\#}} & q_{\#}(\bar{\alpha}) & \longrightarrow 0 \\
 \text{s.t., } (\bar{\alpha} - \partial \bar{A}) \in \text{Ker}(q_{\#}) & & & &
 \end{array} \tag{23}$$

■

Corollary C3. Consider $\bar{\alpha} \in C_{N-1}(\mathbb{R}^D - \tilde{S})$ such that its boundary, $\partial \bar{\alpha}$, is either empty or lies completely in L . Consider the set of all the $(N-1)$ -chains in L with boundary coinciding with $\partial \bar{\alpha}$ (if $\partial \bar{\alpha} = 0$, we consider all $(N-1)$ -cycles in L), and let Q denote the set of $\phi_{\bar{S}}$ -image of those. Then, $[q_{\#}(\bar{\alpha})] = 0 \in H_n(X, L)$ if and only if $\phi_{\bar{S}}(\bar{\alpha}) \in Q$.

Proof.

The statement follows directly from Proposition P6 by setting $X = (\mathbb{R}^D - \tilde{S})$ and $n = N-1$ and by noting that, $\phi_{\bar{S}}(\bar{\alpha} - \iota \circ \bar{\beta}) = 0$ if and only if $[\bar{\alpha} - \iota \circ \bar{\beta}] = 0$. Moreover, due to the linearity of $\phi_{\bar{S}}$, we have $\phi_{\bar{S}}(\bar{\alpha} - \iota \circ \bar{\beta}) = 0 \Rightarrow \phi_{\bar{S}}(\bar{\alpha}) = \phi_{\bar{S}}(\iota \circ \bar{\beta})$. For all computational purpose, ι becomes the identity map since we use a single coordinate chart on $(\mathbb{R}^D - \tilde{S})$. ■

One motivation for considering this kind of spaces arise from frontier-based exploration problems in robotics [18], where L represents the unexplored/unknown region in a configuration space, and the task at hand is to deploy robots, starting from a point in the known/explored region, to reach L following different topological classes. While we do not discuss a complete exploration problem in this paper, we will describe, with example, how optimal trajectories in the different homology classes for reaching L can be obtained using a graph search-based approach. As far as implementation for search-based planning for robot trajectories is concerned, we will mostly be interested in $\bar{\alpha}$

that has empty boundary (formed by trajectories sharing the same start and goal points in $(\mathbb{R}^D - \tilde{\mathcal{O}})$, as shown in). Thus the Q that will be of our interest is the one for $\partial\bar{\alpha} = \emptyset$.

7.1 Search-based Implementation

A graph search-based algorithm, as described earlier, can once again be employed for the case with $N = 2$, for finding optimal trajectories in different homology classes on $(\mathbb{R}^D - \tilde{\mathcal{S}})/L$. Homology classes of trajectories (which are relative chains in $C_1(\mathbb{R}^D - \tilde{\mathcal{S}}, L)$) are defined informally in a way similar to one in Remark 1.

The complete environment, $\mathbb{R}^D - \tilde{\mathcal{O}}$, is discretized to create a graph, \mathcal{G} , as before. Edges of the graph lying in L are assigned zero costs (a small positive value is used in practice for numerical stability), while for ones in the complement space is assigned the costs induced by a metric of choice (we choose the Euclidean metric of the ambient space for the example in Figure 14). The construction of the augmented graph is similar to the construction of $\hat{\mathcal{G}}$ as before, except that now a vertex $\{\mathbf{v}, \mathbf{c}\}$ is identified with $\{\mathbf{v}, \bar{\mathbf{c}}\}$ if $\mathbf{c} - \bar{\mathbf{c}} \in Q$ (where Q is the set corresponding to $\partial\bar{\alpha} = \emptyset$). We call this derived graph $\tilde{\mathcal{G}}$.

Figure 14 shows an environment that is similar to the one illustrated in Figure 10, except that now everything outside a rectangular region containing the two obstacles is considered to be part of L (the , where the metric, and hence the cost of every edge is set to zero). The space under consideration is thus topologically a sphere, with collapsed to a single point. For the search algorithm, we choose the same start coordinate as before (near the bottom of the environment – *almost* symmetrically placed with respect to the two obstacles), but we place the goal vertex inside L (Exact choice does not matter. Although, if there were multiple path-connected components of L , we would have to place one goal vertex in each connected component for exploring all the homology classes).

Figures 14(a)-(e) shows exploration of first 5 homology classes (in order of path lengths) in $(\mathbb{R}^D - \tilde{\mathcal{O}})/L$ by searching in $\tilde{\mathcal{G}}$. However, we notice that in the classes 3 and 5, the parts of the trajectories lying in $(\mathbb{R}^D - \tilde{\mathcal{O}} - L)$ have disconnected components. Notice that it is not possible to alter such trajectories through small variations to make them fall inside $(\mathbb{R}^D - \tilde{\mathcal{O}} - L)$, and still remain close to optimal. This is because we use the Euclidean metric on \mathbb{R}^D for length of the trajectories instead of the round metric on $\mathbb{S}^D \cong \mathbb{R}^D/L$.

While these solutions are technically optimal in the augmented graph, for exploration problems, where computed trajectories are not desired to have multiple connected components, we can alter the search algorithm slightly in order to obtain trajectories as shown in Figures 14(f)-(j) belonging to the same classes, but connected. Instead of searching in $\tilde{\mathcal{G}}$, we first perform a pre-computation step where we execute a Dijkstra's search in the subgraph of \mathcal{G} that lies in L starting from the 'goal' vertex, and compute the value of $\phi_{\tilde{\mathcal{S}}}$ up to every other vertex in the subgraph following some path lying inside L (and its boundary, ∂L). Let us represent that computed value corresponding to vertex $\mathbf{v}_L \in \mathcal{V}|_L$ by $p(\mathbf{v}_L)$. The main search is then performed using Dijkstra's algorithm in the subgraph of $\hat{\mathcal{G}}$ with vertices lying inside $(\mathbb{R}^D - \tilde{\mathcal{O}} - L)$ (and the boundary, ∂L), starting from the 'start' vertex, and expanding vertices until the boundary between L and $(\mathbb{R}^D - \tilde{\mathcal{O}} - L)$ are reached. In addition, a vertex on the boundary, $\{\mathbf{v}'_L, \mathbf{c}\}$, is identified with $\{\mathbf{v}''_L, \bar{\mathbf{c}}\}$ if $((\mathbf{c} - p(\mathbf{v}'_L)) - (\bar{\mathbf{c}} - p(\mathbf{v}''_L))) \in Q$.

One interesting observation in the result of Figure 14 is that apparently the search does not return any trajectory that winds around the obstacle on the right. This is because on $(\mathbb{R}^D - \tilde{\mathcal{O}})/L$ (i.e. the sphere punctured by the two obstacles), a trajectory connecting the two chosen points that wind around one obstacle can be deformed over the sphere to make it wind around the other obstacle – making them homotopic, and hence homologous. This is illustrated in Figure 14(k). The reason that the obstacle on the left gets preference in the result of the search algorithm is because the start

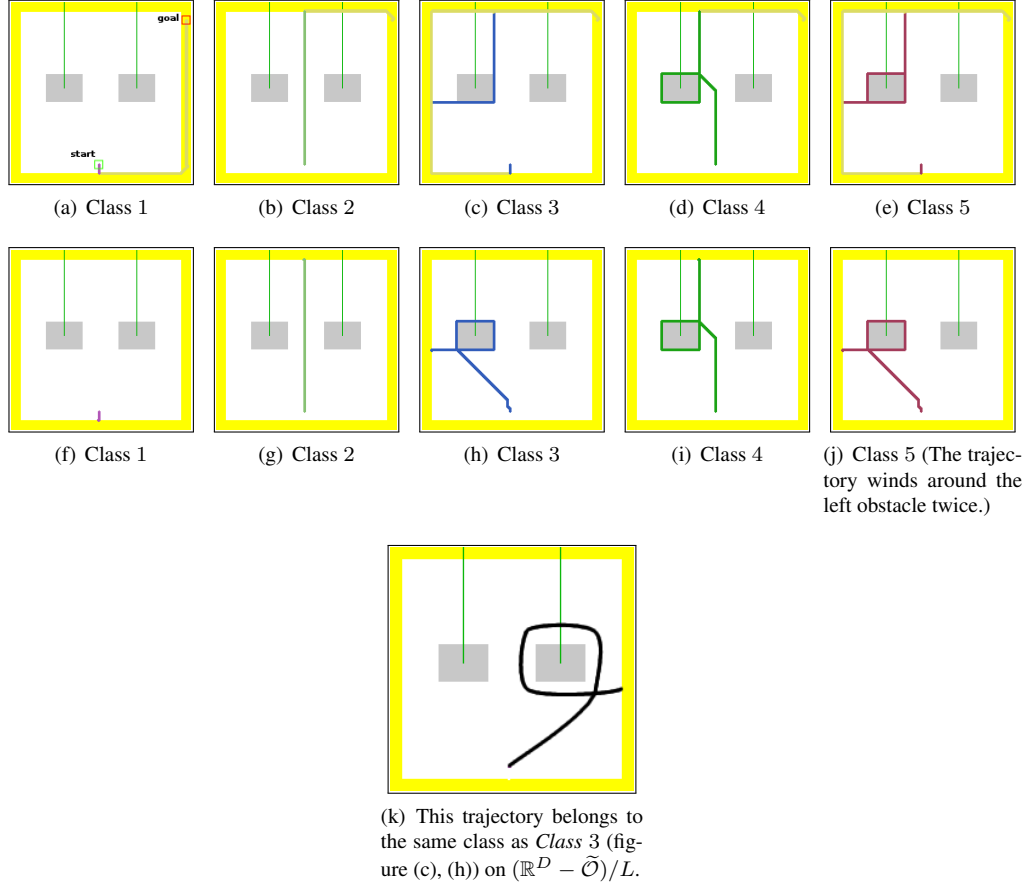


Figure 14: The shown in the figures is L , which we *collapse* to a single point. The gray rectangles are the obstacles. (a)-(e): The first 5 homology classes of trajectories in $(\mathbb{R}^D - \tilde{\mathcal{O}})/L$ connecting a given start point in $(\mathbb{R}^D - \tilde{\mathcal{O}} - L)$, and an arbitrarily chosen point in L (exact choice does not matter since we mod out L , which has a single path connected component) found using graph search algorithm in $\hat{\mathcal{G}}$. (f)-(j): The solutions obtained using modified algorithm to ensure that the trajectories have single connected components in $(\mathbb{R}^D - \tilde{\mathcal{O}} - L)$.

coordinate is located slightly closer (by 1 discretization unit) to the obstacle on the left than one on the right.

8 Conclusion

The problem of optimal path planning (and its higher-dimensional generalizations to homology H_N) has as prerequisite homology cycle planning. We have addressed this precursor in the context of obstacle-punctured Euclidean spaces. The novel features of this work involve (1) the skeletal restructuring of the obstacles $\tilde{\mathcal{O}}$ to facilitate (2) the design of a set of explicit cocycles for a complete set of invariants for the homology class of the cycles. In this, the language of de Rham cohomology is the critical technical step, using integration of differential forms over cycles. We have demonstrated the use of our methods for solving homologically-constrained optimal path planning problems in robotics, and topological exploration of robot configuration spaces. A further generalization allowed us to achieve similar objectives in ambient spaces that are not Euclidean, at the expense of an increased computational complexity. Further work is needed to address this issue.

Acknowledgements

We gratefully acknowledge support from the ONR Antidote MURI project, grant no. N00014-09-1-1031.

References

- [1] William E. Baylis. *Clifford (Geometric) Algebras With Applications in Physics, Mathematics, and Engineering*. Birkhuser Boston, 1 edition, 1996.
- [2] Subhrajit Bhattacharya. A template-based c++ library for large-scale graph search and planning, 2011. See <http://subhrajit.net/index.php?WPAGE=yagsbpl>.
- [3] Subhrajit Bhattacharya, Maxim Likhachev, and Vijay Kumar. Topological constraints in search-based robot path planning. *Autonomous Robots*, pages 1–18, June 2012. DOI: 10.1007/s10514-012-9304-1.
- [4] R. Bott and L.W. Tu. *Differential Forms in Algebraic Topology*. Graduate texts in mathematics. Springer-Verlag, 1982.
- [5] Frederic Bourgault, Alexei A. Makarenko, Stefan B. Williams, Ben Grocholsky, and Hugh F. Durrant-Whyte. Information based adaptive robotic exploration. In *in Proceedings IEEE/RSJ International Conference on Intelligent Robots and Systems (IROS)*, pages 540–545, 2002.
- [6] T. H. Cormen, C. E. Leiserson, R. L. Rivest, and C. Stein. *Introduction to algorithms*. MIT Press, 2nd edition, 2001.
- [7] A. Dold. *Lectures on algebraic topology*. Classics in mathematics. Springer, 2nd edition, 1995.
- [8] Dave Ferguson, Thomas Howard, and Maxim Likhachev. Motion planning in urban environments. *Journal of Field Robotics*, 25(11-12):939–960, 2008.

- [9] Harley Flanders. *Differential Forms with Applications to the Physical Sciences*. Dover Publications, New York, 1989.
- [10] Mark Galassi, Jim Davies, James Theiler, Brian Gough, Gerard Jungman, Michael Booth, and Fabrice Rossi. *Gnu Scientific Library: Reference Manual*. Network Theory Ltd., February 2003.
- [11] R. Ghrist and S. LaValle. Nonpositive curvature and pareto optimal motion planning. *SIAM Journal of Control and Optimization*, 45, 2006.
- [12] P. E. Hart, N. J. Nilsson, and B. Raphael. A formal basis for the heuristic determination of minimum cost paths. *IEEE Transactions on Systems, Science, and Cybernetics*, SSC-4(2):100–107, 1968.
- [13] Allen Hatcher. *Algebraic Topology*. Cambridge University Press, 2001.
- [14] S. Koenig and M. Likhachev. D* Lite. In *Proceedings of the Eighteenth National Conference on Artificial Intelligence (AAAI)*, pages 476–483, 2002.
- [15] Conrad Sanderson. Armadillo: An open source c++ linear algebra library for fast prototyping and computationally intensive experiments. Technical report, NICTA, 2010.
- [16] H. Seifert, W. Threlfall, J.S. Birman, and J. Eisner. *Seifert and Threlfall, A textbook of topology*. Pure and applied mathematics. Academic Press, 1980.
- [17] A. Stentz and M. Hebert. A complete navigation system for goal acquisition in unknown environments. *Autonomous Robots*, 2(2):127–145, 1995.
- [18] Sebastian Thrun, Wolfram Burgard, and Dieter Fox. *Probabilistic Robotics (Intelligent Robotics and Autonomous Agents)*. The MIT Press, 2005.
- [19] Yan Zhou, Bo Hu, and Jianqiu Zhang. Occlusion detection and tracking method based on bayesian decision theory. In Long-Wen Chang and Wen-Nung Lie, editors, *Advances in Image and Video Technology*, volume 4319 of *Lecture Notes in Computer Science*, pages 474–482. Springer Berlin / Heidelberg, 2006.